J. Fluid Mech. (1995), *vol.* 284, *pp.* 63–96
Copyright © 1995 Cambridge University Press

Upstream influence and the form of standing hydraulic jumps in liquid-layer flows on favourable slopes

By ROBERT I. BOWLES

Department of Mathematics, University College London, Gower Street, London WC1E 6BT, UK

(Received 7 July 1993 and in revised form 8 June 1994)

Steady planar flow of a liquid layer over an obstacle is studied for favourable slopes. First, half-plane Poiseuille flow is found to be a non-unique solution on a uniformly sloping surface since eigensolutions exist which are initially exponentially small far upstream. These have their origin in a viscous–inviscid interaction between the retarding action of viscosity and the hydrostatic pressure from the free surface. The cross-stream pressure gradient caused by the curvature of the streamlines also comes into play as the slope increases. As the interaction becomes nonlinear, separation of the liquid layer can occur, of a breakaway type if the slope is sufficiently large. The breakaway represents a hydraulic jump in the sense of a localized relatively short-scaled increase in layer thickness, e.g. far upstream of a large obstacle. The solution properties give predictions for the shape and structure of hydraulic jumps on various slopes. Secondly, the possibility of standing waves downstream of the jump is addressed for various slope magnitudes. A limiting case of small gradient, governed by lubrication theory, allows the downstream boundary condition to be included explicitly. Numerical solutions showing the free-surface flow over an obstacle confirm the analytical conclusions. In addition the predictions are compared with the experimental and computational results of Pritchard *et al.* (1992), yielding good qualitative and quantitative agreement. The effects of surface tension on the jump are also discussed and in particular the free interaction on small slopes is examined for large Bond numbers.

1. Introduction

The standing hydraulic jump, formed when a liquid layer adjusts abruptly ahead of an obstacle, has been the subject of much study and is of importance in civil engineering and the chemical industry, as well as being a fascinating phenomenon in its own right (see the works of Rayleigh 1914; Lamb 1932; Lighthill 1978). Until recently the jump has usually been treated as a discontinuity in the flow, with the internal structure ignored. Nevertheless, it has long been realized that the jump can take many different forms, be it two-dimensional or axisymmetric, incorporating for example separation from the bed, a roller at the free surface, waves downstream or all of these: see Larras (1962), Watson (1964), Clarke (1970), Peregrine (1974), Craik *et al.* (1981), da Silva & Peregrine (1988). An important step forward in understanding this internal structure was made by Gajjar & Smith (1983) who derive boundary-layer equations describing the jump on a uniform velocity profile at high Reynolds number (see also Brotherton-Ratcliffe 1986). The dominant physics is an interplay, a so-called

viscous–inviscid interaction, between the hydrostatic pressure generated by the free-surface displacement and viscous effects in a sublayer at the wall. The flow can separate owing to the strong adverse pressure gradient caused by the rapidly increasing depth of the layer. Beyond, the free surface develops a blunt, approximately parabolic, shape. This is not unlike the axisymmetric hydraulic jumps measured experimentally by Craik *et al.* (1981) in which a falling jet of water strikes a horizontal plate, spreads radially, undergoes a jump and subsequently falls off the edge of the plate. Bowles & Smith (1992, which we will refer to as BS) extend the work of Gajjar & Smith (1983) and investigate the internal structure of the jump in fully developed flow on a horizontal surface and show that at large Froude numbers the flow is governed by the interactive boundary-layer equations (cf. Bowles 1990 on other Froude numbers). They incorporate effects of surface tension leading to encouraging quantitative comparison with these experiments.

The pressure (P) driving the interactive boundary-layer equations is not prescribed as in the classical boundary-layer equations. Instead it is related to the boundary-layer displacement ($-A$) via a so-called pressure-displacement ($P-A$) law (Stewartson 1974, 1982; Smith 1982). For certain $P-A$ laws, including those relevant here, the boundary-layer equations are rendered elliptic by this interaction. This manifests itself in eigensolutions which are initially exponentially small upstream but which develop nonlinearly downstream (Lighthill 1953). This development is usually of two types. The pressure may increase, possibly leading to separation (a compressive interaction) or it may decrease, leading perhaps to a finite-distance singularity in the solution (an expansive interaction). These are known as free interactions. The initial amplitude of the eigensolution is dependent on the downstream boundary condition and if this condition is included the problem is described as a forced interaction. Typically, as the size of the disturbance increases, the forced solutions exhibit a free interaction far upstream.

The position of the jump is not predicted by BS although they do indicate that viscous effects play a vital role in determining the structure and position of the jump in the experiments. The complete flow, apart from small regions about the jet and the edge of the plate, is governed by the interactive boundary-layer equations presented in BS with viscous effects felt across the depth of the layer. This has been realized by Bohr, Dimon & Putkaradze (1993) who treat the equations for the axisymmetric problem approximately, obtaining predictions for the jump radius by assuming that the flow downstream is governed by lubrication theory, with the effects of inertia reduced by the thickening of the flow as it passes through the jump. The jump itself is treated as a discontinuity. More recently Higuera (1994) has treated the two-dimensional problem numerically. He obtains solutions for the entire flow including a region of rapid adjustment with a near-parabolic free-surface profile which emerges as the Froude number increases. He also investigates this limit analytically, expanding upon the work of BS, showing how the separated flow reattaches, and that the flow downstream of the jump is indeed governed by lubrication theory. With this knowledge an expression for the variation of the jump position and strength with Froude number is obtained.

This paper concentrates on the interactive boundary-layer equations relevant to planar liquid-layer flow on a sloping surface. This work was originally undertaken as a preliminary to a study of the problem on a horizontal surface which has since been solved as described above. The advantage of this study is that the far-field boundary condition is of half-Poiseuille flow representing a balance of the viscous and the gravitational effects. This also implies that the Froude number is proportional to the product of the slope and the Reynolds number and is not a free parameter. The

corresponding problem for flow on a horizontal surface does not have a suitable solution at infinity, as this balance is not attainable. Instead the flow field is determined by insisting that the expansive singularity (Brown, Stewartson & Williams 1974; Bowles 1990; Bohr *et al.* 1992; Daniels 1992; Higuera 1994), occurs at the plate edge. The present work differs from Gajjar & Smith (1983) in that it is concerned with fully developed flow, and from BS, in that we study the form of the free interaction on a variety of slopes, corresponding to different Froude numbers. In addition we study forced interactions.

We denote the slope by $\tan\alpha^*$ and define a Reynolds number, Re based on the volume flux per unit width of the layer. The investigation is primarily concerned with slopes of $O(Re^{-1})$, discussed in §4. On these slopes the prescribed pressure gradient due to the slope is comparable with the self-induced pressure gradient caused by a thickening or thinning of the layer due to viscous influences. These act across the layer's depth on a long $O(Re)$ lengthscale. For slopes much less than this, studied in detail in §5, the development is still slower, inertia is unimportant and the flow is described by lubrication theory.

The lubrication approximation has been used by many authors to derive equations governing the behaviour of liquid films. One of the first was Moffatt (1977). Huppert (1982*a*,*b*) uses it to study the spreading of a fixed volume of fluid on a surface. See also Lister (1992). Wilson & Jones (1983) study the fall of a thin liquid film down a vertical wall into a pool. In this case, since the wall is vertical, the gravitational contributions to the pressure are unimportant and surface tension dominates. See also Christodoulou & Scriven (1989), Higgins & Scriven (1979) and Tuck & Schwartz (1990). All these authors concentrate on the case where the self-induced gravitational pressure gradient is negligible or the mass of fluid is fixed. Here in contrast we are interested in the effects of the self-induced pressure gradient and flows which asymptote to some constant depth at infinity. There is a strong connection with the work of Chester (1966), who uses lubrication theory to give a description of a viscosity-dominated bore, or moving hydraulic jump, travelling downstream. Lubrication theory is used in the present context by Pritchard, Scott & Tavener (1992, which we shall refer to as PST) who, in independent work, derive the ordinary differential equation for the layer depth and solve it numerically in a particular case. Here we examine the equation in some detail, interpreting its solutions in terms of free and forced viscous–inviscid interactions and using these to give predictions for the form of forced interactions on the larger slopes.

For slopes large on the $O(Re^{-1})$ scaling the streamwise development is fast so that viscous effects are concentrated near to the bed leading to a multistructured double-deck description of the flow. For slopes of this magnitude the Froude number, based on the depth far upstream, is large and the flow largely supercritical. Upstream propagation of waves is only possible in a viscous sublayer close to the wall, where owing to the no-slip boundary condition, the flow is locally subcritical. Viscous effects act on these waves reducing their amplitude rapidly so that, in the steady flows we study here, the upstream-influence lengthscale, i.e. the streamwise extent of the adjustment is small. On slopes of this magnitude the flow undergoes breakaway separation (i.e. the main body of the oncoming velocity profile detaches from the bed) and the layer increases in thickness over a relatively short scale. We interpret this type of interaction as a hydraulic jump. To describe the slower interactions on the shallower slopes where the Froude number is not so large we shall use the word 'adjustment'.

For slopes as large as $O(Re^{-5/7})$ the development is so rapid that the cross-stream pressure gradient caused by streamline curvature may no longer be neglected. In addition the self-induced pressure gradient dominates over the gradient due to the

slope. Slopes of this magnitude have been discussed by Gajjar (1987). We discuss them only briefly here, extending the $P-A$ law to include the prescribed pressure gradient due to the slope. Gajjar (1987) shows that eigensolutions exist and gives analytical and numerical solutions for flow over a convex corner which exhibit waves just downstream of the corner. We also study the stationary wave train which may occur downstream of a jump, again from the standpoint of interactive boundary-layer theory. An increase in the normalized wavelength of these waves with increasing slope is predicted.

This work is primarily concerned with the following themes. First, in §2 we show the non-uniqueness of the half-Poiseuille flow of a planar liquid layer on a favourable slope through the streamwise growth of initially small eigensolutions.

Secondly, in §§3 and 4 we investigate the structure and nonlinear development of these eigensolutions for different slope magnitudes at large Re. We discuss the implication this has for the shape of hydraulic jumps as the dominant physics governing these eigensolutions alters. We find that, for all slopes, the flow far downstream has a horizontal free surface and we examine the flow beneath the surface. Specifically we ask two questions: (*a*) whether the flow adjusts so that the free-surface remains concave upwards or whether a region in which the free surface is convex upwards is to be expected; and (*b*) whether or not the flow separates from the bed. In answer to (*a*), we find that the latter behaviour is to be expected only on slopes that are neither too small nor too large, $1.814Re^{-1} < \alpha^* \ll Re^{-1/7}$. The flow separates if the slope is sufficient large, $\alpha^* > 4.712Re^{-1}$.

Thirdly, we are interested in the position of the jump upstream of a large obstacle mounted on the slope. Since the ultimate downstream form of the free interactions has a horizontal free surface and we expect the free interaction to occur far upstream of a large obstacle we deduce that the jump will occur at an upstream distance proportional to the obstacle height. In §5 we show this analytically for solutions valid for slopes small on the $O(Re^{-1})$ scale, and numerically for slopes of $O(Re^{-1})$ in §6. In particular, for slopes large on this scale, we identify two scales for the motion – the shortened scales of the jump far upstream and the longer scales over which the flow negotiates the obstacle itself.

Fourthly, also in §6, we make a comparison with the predictions of this work on jump shape and position with the numerical and experimental results of PST, with good agreement on many points.

Finally, throughout the paper, we briefly discuss the effect surface tension has on the development of the eigensolution. In particular, in Appendix B, we examine the free interaction on small slopes in the limit of large Bond number and show that it takes the form of a wave train upstream of a final dip in the free surface followed by an approach of the free surface to the horizontal.

2. The governing equations and the departure from half-Poiseuille flow

2.1. *The equations governing the first stages of the departure*

Consider a uniform slope of angle α^* to the horizontal. Let x^*, y^* measure distance parallel and normal to the slope respectively, with $y^* = 0$ coinciding with the surface. A film of viscous incompressible fluid runs down the slope in such a way that it remains two-dimensional. Far upstream the fluid has depth h^*, and the volume flux of fluid per unit width is Q^*. We choose to normalize length, fluid velocity, and pressure with h^*, Q^*/h^* and $\rho g h^*$, where ρ is the density of the fluid and g is the acceleration due to gravity which acts vertically downwards. We introduce the Reynolds number, $Re = Q^*/\nu$, where ν is the kinematic viscosity of the fluid, and the Froude number,

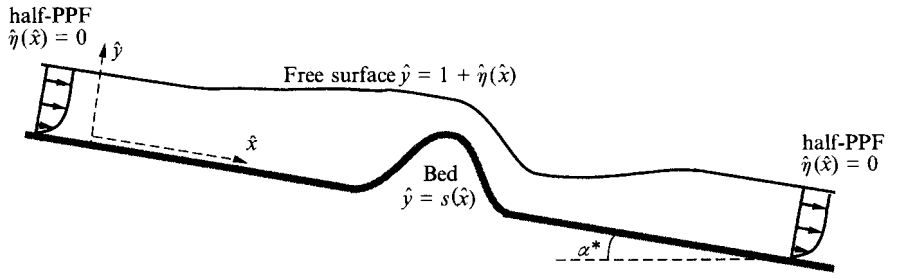

FIGURE 1. The problem in non-dimensional terms illustrating the coordinates, $\hat{x}$, $\hat{y}$, the free surface $\hat{y} = 1 + \hat{\eta}$ and the bed $\hat{y} = s(\hat{x})$, defined in §2.1.

$Fr = Q^{*2}/(gh^{*3})$. Normalized distances and velocities parallel and normal to the slope respectively are $\hat{x}$, $\hat{y}$, and $\hat{U}$, $\hat{V}$. The normalized pressure and depth are written as $\hat{P} - \cos\alpha^*(\hat{y} - 1)$ and $1 + \hat{\eta}$. The pressure and fluid stresses are taken to be zero in the air above the liquid layer and the governing equations and boundary conditions reduce to

$$\hat{U}\hat{U}_{\hat{x}} + \hat{V}\hat{U}_{\hat{y}} = (-\hat{P}_{\hat{x}} + \sin\alpha^*)\, Fr^{-1} + Re^{-1}(\hat{U}_{\hat{y}\hat{y}} + \hat{U}_{\hat{x}\hat{x}}), \tag{2.1a}$$

$$\hat{U}\hat{V}_{\hat{x}} + \hat{V}\hat{V}_{\hat{y}} = -\hat{P}_{\hat{y}}\, Fr^{-1} + Re^{-1}(\hat{V}_{\hat{y}\hat{y}} + \hat{V}_{\hat{x}\hat{x}}), \tag{2.1b}$$

$$\hat{U}_{\hat{x}} + \hat{V}_{\hat{y}} = 0, \quad \int_0^{1+\hat{\eta}} \hat{U}\, \mathrm{d}\hat{y} = 1, \tag{2.1c, d}$$

$$\hat{U} = \hat{V} = 0 \quad \text{at} \quad \hat{y} = 0, \tag{2.1e, f}$$

and, at the free surface, $\hat{y} = 1 + \hat{\eta}(x)$,

$$(\hat{U}_{\hat{x}} - \hat{V}_{\hat{y}})\,\hat{\eta}_{\hat{x}} + \tfrac{1}{2}(\hat{U}_{\hat{y}} + \hat{V}_{\hat{x}})(1 - \hat{\eta}_{\hat{x}})^2 = 0, \tag{2.2a}$$

$$\hat{P} - \cos\alpha^*\hat{\eta} = \frac{2Fr}{Re}[\hat{U}_{\hat{x}}\,\hat{\eta}_{\hat{x}}^2 - (\hat{U}_{\hat{y}} + \hat{V}_{\hat{x}})\,\hat{\eta}_{\hat{x}} + \hat{V}_{\hat{y}}]\frac{1}{1 + \hat{\eta}_{\hat{x}}^2} - B\frac{\hat{\eta}_{\hat{x}\hat{x}}}{(1 + \hat{\eta}_{\hat{x}}^2)^{3/2}}, \tag{2.2b}$$

$$\hat{U}\hat{\eta}_{\hat{x}} = \hat{V}, \tag{2.2c}$$

where $B = T/(\rho g h^{*2})$ is a Bond number and T the coefficient of surface tension at the fluid–air interface.

Far upstream the flow is half-Poiseuille, $\hat{U}(\hat{y}) = U_{PPF}(\hat{y}) = 3(\hat{y} - \hat{y}^2/2)$, $\hat{V} = 0$ and the reduced pressure $\hat{P}$ is equal to zero. Viscous dissipation balances gravity parallel to the slope giving

$$Re\sin\alpha^* = 3Fr, \tag{2.3}$$

or, in dimensional terms, $h^{*3} = 3Q^*\nu/(g\sin\alpha^*)$. We define a stream function, $\hat{\psi}(\hat{x}, \hat{y})$ such that $\hat{U} = \hat{\psi}_{\hat{y}}$ and $\hat{V} = -\hat{\psi}_{\hat{x}}$. Far upstream $\hat{\psi} = F(\hat{y}) = 3(\hat{y}^2/2 - \hat{y}^3/6)$. If an obstacle is mounted on the slope then (2.1*e*) and (2.1*f*) are to be applied at $\hat{y} = s(\hat{x})$ and the lower limit of integration in (2.1*d*) is $s(\hat{x})$ where $s(\hat{x})$ represents the obstacle. See figure 1.

We consider perturbations to this flow which are exponentially small far upstream, linearizing about the Poiseuille profile and seeking solutions of the form

$$\hat{\psi} = F(\hat{y}) + a\exp(\hat{q}\hat{x})f(\hat{y}), \quad \hat{\eta} = a\exp(\hat{q}\hat{x}). \tag{2.4a, b}$$

Substitution into (2.1) yields the system

$$(\hat{q}a)[F'f' - fF''] = -\hat{P}_{\hat{x}}\, Fr^{-1} + a\, Re^{-1}(f'''' + \hat{q}^2 f'), \tag{2.5a}$$

$$-\hat{q}^2 aF'f = -\hat{P}_{\hat{y}}\, Fr^{-1} - \hat{q}a\, Re^{-1}(f'' + \hat{q}^2 f), \tag{2.5b}$$

where the prime represents $\partial/\partial\hat{y}$. We write $\hat{P} = \cos\alpha^* a \exp(\hat{q}\hat{x})\,\Pi(\hat{y})$, and use (2.3), giving

$$\hat{q}\left(F'f' - fF'' + \frac{3\Pi}{Re\tan\alpha^*}\right) = Re^{-1}(f''' + \hat{q}^2 f'), \tag{2.6a}$$

$$\Pi' = \frac{\tan\alpha^* Re\,\hat{q}^2}{3} F'f - \frac{\tan\alpha^*\hat{q}}{3}(f'' + \hat{q}^2 f), \tag{2.6b}$$

with boundary conditions

$$f(0) = f'(0) = 0, \tag{2.6c,d}$$

$$f(1) = -\tfrac{3}{2}, \quad f''(1) - \hat{q}^2 f(1) = 3, \quad \Pi(1) = 1 - 2\hat{q}\tan\alpha^* f'(1)/3 - B\hat{q}^2/\cos\alpha^* \tag{2.6e–g}$$

from linearizing about the position of the free surface $\hat{y} = 1$. It is worthwhile identifying the origins of the terms in (2.6). The left-hand side of (2.6*a*) represents streamwise inertial and pressure forces, balanced by viscous effects on the right. The pressure variation across the layer is shown by (2.6*b*) to be made up of the effects of streamline curvature (first term on the right-hand side) and viscous effects (second term). Surface tension enters through the boundary condition on Π. The system represents an eigenvalue problem for the growth rate $\hat{q}$ which must be positive. The amplitude of the perturbation, a, is arbitrary. We consider (2.6) in the limit of large Reynolds number for progressively steeper slopes.

2.2. *Slopes of* $O(Re^{-1})$

If the slope is $O(Re^{-1})$ we write $\tan\alpha^* = Re^{-1}\alpha$, $\hat{q} = q\,Re^{-1}$, so that the lengthscale of the motions is $\hat{x} \sim O(Re)$ and the Froude number is $\alpha/3$ and is $O(1)$. These scalings preserve a balance between viscous, pressure and inertial effects across the layer. In this limit (2.6) reduces to $\Pi = 1$ for all $\hat{y}$ (for order-one Bond number), and

$$q(F'f' - fF'' + 3/\alpha) = f''', \tag{2.7a}$$

$$f''(1) = 3, \quad f(1) = -\tfrac{3}{2}, \quad f(0) = f'(0) = 0. \tag{2.7b–e}$$

Numerical solutions to this problem, obtained by the use of finite differences and checked for grid independence, are presented in figure 2 showing the single positive value of q as a function of α, together with asymptotic results derived below. There are many negative values of q for a given α. As $\alpha \to 0$, q approaches zero, corresponding to a further lengthening of the scale for the disturbance but as $\alpha \to \infty$, q increases rapidly.

For small α the predominant balance is one between viscosity and pressure. We find that $q \sim 3\alpha$ and $f \sim 3(\hat{y}^3/2 - \hat{y}^2) = -\hat{y}F'$. The stream function can be written as $\hat{\psi} = F - a\exp(\hat{q}\hat{x})\hat{y}F' = F(\hat{y}(1 - a\exp(\hat{q}\hat{x})))$. Thus the flow is still half-Poiseuille but thickens for $a > 0$ and thins for $a < 0$. The adjustment occurs on a sufficiently long lengthscale, $\hat{x} \sim O(Re\,\alpha^{-1})$, that viscosity is able to maintain the half-Poiseuille profile.

In the limit of large α, moving towards gradients larger than $O(Re^{-1})$, the solution has a double-deck form. Examining (2.7*a*) for large q and α, we note that the inertial terms dominate for $\hat{y}$ of $O(1)$ with the pressure term reduced by the size of α. The solution here is $f = -F'$. Thus there is a slip velocity at the wall of magnitude -3. This is reduced to zero in a boundary layer of thickness $\hat{y} \sim O(\delta)$, say, where f and the unperturbed flow F' (which asymptotes $3\hat{y}$ as $\hat{y} \to 0$) are also $O(\delta)$. The viscous, pressure and inertial terms of (2.7*a*) in this layer are of sizes $O(\delta^{-2})$, $O(q\alpha^{-1})$ and $O(q\delta)$

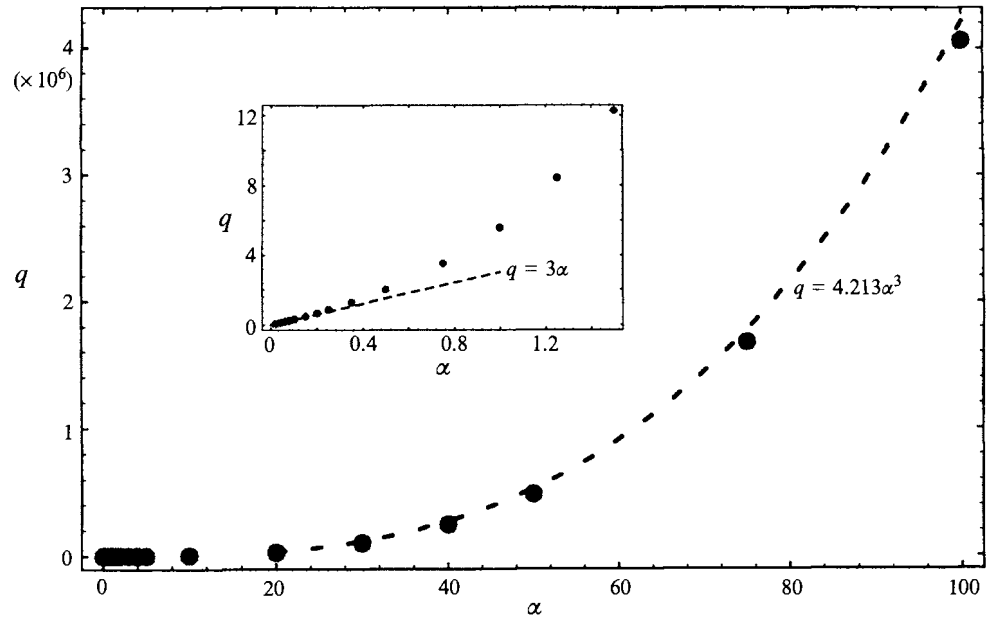

FIGURE 2. The eigenvalue q satisfying (2.7*a*) as a function of α, the scaled slope. The disks represent values obtained numerically with the results for small values of α illustrated in the inset. The dashed lines are the asymptotes $q = 3\alpha$ as $\alpha \to 0$ and $q = 4.213\alpha^3$ as $\alpha \to \infty$.

respectively so that a balance is achieved if $q \sim O(\alpha^3)$, $\delta = \alpha^{-1}$. We write $q = \alpha^3 \bar{q}$, $\hat{y} = \alpha^{-1}\bar{z}$, $f_{\hat{y}} = \alpha^{-1}\bar{u}$, where $\bar{q}$, $\bar{z}$ and $\bar{u}$ are $O(1)$ as $\alpha \to \infty$, and the governing equations become

$$3\bar{q}(\bar{z}\bar{u} + \bar{v}) = -3\bar{q} + \bar{u}_{\bar{z}\bar{z}}, \quad \bar{u} + \bar{v}_{\bar{z}} = 0, \tag{2.8a, b}$$

$$\bar{u} = \bar{v} = 0 \quad \text{at} \quad \bar{z} = 0, \quad \bar{u} \to -3 \quad \text{as} \quad \bar{z} \to \infty. \tag{2.8c–e}$$

We find $\bar{q} = 9(3\,|\mathrm{Ai}'(0)|)^3$, where Ai is the usual Airy function, giving

$$q \sim 4.213\alpha^3. \tag{2.9}$$

2.3. *Slopes of $O(Re^{-5/7})$ and greater*

The relative error in neglecting the transverse pressure gradient generated by the streamline curvature is $O(\alpha^7 Re^{-2})$. This becomes $O(1)$ if $\alpha = O(Re^{2/7})$, or $\tan\alpha^* = \tilde{\alpha} Re^{-5/7}$, say, with $\tilde{\alpha} = O(1)$. The Froude number for these flows is $Re^{2/7}\tilde{\alpha}/3$ from (2.3) and is large. From Gajjar (1987) we note the lengthscale for the development of the flow to be $O(Re^{1/7})$ and that viscous effects are confined to a sublayer of thickness $O(Re^{-2/7})$ at the bed, because of the relatively rapid development of the flow. We write $q = \tilde{q} Re^{-1/7}$ with $\tilde{q} = O(1)$. In this case, where $y = O(1)$, (2.6) becomes

$$\Pi' = \frac{\tilde{\alpha}\tilde{q}^2}{3} F' f, \quad F'f - fF'' = 0, \tag{2.10a, b}$$

with boundary conditions (2.7*b–d*) and $\Pi(1) = 0$, neglecting surface tension. Again $f = -F'$, giving a slip velocity of -3 at the wall. In addition

$$\Pi(1) - \Pi(0) = -\frac{\tilde{\alpha}\tilde{q}^2}{3} \int_0^1 F'^2 \,\mathrm{d}\bar{y}. \tag{2.11a}$$

Since the basic flow is of a half-Poiseuille type this, gives

$$\Pi(0) = 1 + \tfrac{2}{5}\tilde{\alpha}\tilde{q}^2. \tag{2.11b}$$

The addition of the second term in (2.11*b*) is the only new effect so in the viscous sublayer the governing equations are (2.8) with $-3\tilde{q}(1+\frac{2}{5}\tilde{\alpha}\tilde{q}^2)$ replacing $-3\bar{q}$ on the right-hand side of (2.8*a*). We find, as does Gajjar (1987), that $\tilde{q}(1+2\tilde{\alpha}\tilde{q}^2/5)^3 = 9\tilde{\alpha}^3(3|\mathrm{Ai}'(0)|)^3$, which has a real positive root for all $\tilde{\alpha}$.

As $\tilde{\alpha}$ increases, the effects of streamline curvature dominate over those of gravity and the growth rate levels off at $O(Re^{-1/7})$ with $\tilde{q} \sim 9^{1/7}(15|\mathrm{Ai}'(0)|/2)^{3/7}$. This description remains valid for $O(1)$ values of α^*. We conclude that the departure of the flow from half-Poiseuille flow on anything other than shallow slopes is governed by an interaction between streamline curvature in the main part of the liquid layer and viscosity at work in a boundary layer close to the bed.

3. The subsequent development of the pertubations and the shape of hydraulic jumps

We postpone until the next section a description of the nonlinear development of the initially exponentially small perturbations on slopes of $O(Re^{-1})$. Here we examine slopes larger than this on which the development occurs relatively rapidly and takes the form of a jump in the depth of the layer over some shortened lengthscale.

We first consider slopes large on the $O(Re^{-1})$ scale, whose initial development is governed by (2.8). This system is a linearized form of the interactive boundary-layer equations. We formulate a double-deck interactive structure governing the nonlinear development according to (2.1) and (2.2) on slopes of magnitude $O(Re^{-1}\alpha)$ for large α and Re (see BS for more details). The viscous sublayer in which (2.8) holds becomes nonlinear when the perturbation grows to be of size $O(\alpha^{-1})$. The development occurs over the $O(Re\,\alpha^{-3})$ lengthscale identified above and we write $\hat{x} = Re\,\alpha^{-3}\bar{X}$. Just as for the linear case inertia dominates for $\hat{y}$ of $O(1)$ where the perturbation to the oncoming basic half-Poiseuille flow is relatively small. The solution here is $\hat{U} = U_{PPF}(\hat{y}+\alpha^{-1}\bar{A}(\bar{X}))$, $\hat{V} = -\alpha^2 Re^{-1}\bar{A}_{\bar{X}}\,U_{PPF}(\hat{y}+\alpha^{-1}\bar{A}(\bar{X}))$, to first order in α^{-1} where $\bar{A}$ is unknown. This perturbation of $O(\alpha^{-1})$ in the velocity alters the position of the free surface and we write $\hat{\eta} = \alpha^{-1}e$ so that from (2.1*d*) and (2.2*b*) $e = -\bar{A}$ and $\hat{P} = \alpha^{-1}e = -\alpha^{-1}\bar{A} = \alpha^{-1}\bar{\mathrm{P}}$ say (for $O(1)$ Bond number) so that $\bar{P} = -\bar{A}$ at the free surface. From (2.1*b*) $\bar{P}_{\hat{y}} \sim -(\alpha\,Fr)\,\hat{U}\hat{V}_{\hat{x}} = O(\alpha^7 Re^{-2})$ which we assume to be small so that $\bar{P} = -\bar{A}$ at $\hat{y} = 0$. There is also a slip velocity at the wall of size $\alpha^{-1}\lambda\bar{A}$ where $U_{PPF} \sim \lambda\hat{y}$ as $\hat{y} \to 0$ with $\lambda = 3$. The viscous/pressure/inertia balance in the sublayer, where we write $\hat{y} = \alpha^{-1}\bar{Y}$, $\hat{U} = \alpha^{-1}\bar{U}$ and $\hat{V} = \alpha^3\bar{V}$, is governed by

$$\bar{U}\bar{U}_{\bar{X}} + \bar{V}\bar{U}_{\bar{Y}} = -\bar{P}_{\bar{X}} + \bar{U}_{\bar{Y}\bar{Y}}, \quad \bar{U}_{\bar{X}} + \bar{V}_{\bar{Y}} = 0, \tag{3.1a, b}$$

$$\bar{U} = \bar{V} = 0 \quad \text{at} \quad \bar{Y} = 0, \qquad \bar{U} \to \bar{Y} + \bar{A} \quad \text{as} \quad \bar{Y} \to \infty, \tag{3.1c–e}$$

$$\bar{A} \to 0 \quad \text{as} \quad \bar{X} \to -\infty, \quad \bar{P} = -\bar{A}. \tag{3.1f, g}$$

We have made two further normalizations, factoring out firstly the value of λ and secondly the 3 multiplying the pressure term which arises from the relation $Fr^{-1} = 3/\alpha$, by scaling $[\bar{U}, \bar{V}, \bar{P}, \bar{A}, \bar{Y}, \bar{X}]$ with $[3\lambda^{-1}, 3^{-1}\lambda^3,\ 3\lambda^{-2}, 3\lambda^{-2}, 3\lambda^{-2}, 3^3\lambda^{-5}]$. The prescribed pressure gradient adds a term $3^2\alpha^{-1}\lambda^{-3}$ to the right-hand side of (3.1*a*) which is neglected. Equations (3.1) are the nonlinear interactive boundary-layer equations with the $P-A$ law $P = -A$. They have been studied in depth by Gajjar & Smith (1983). Far

upstream on these scales, i.e. as $\bar{X} \to -\infty$, $\bar{A}$ decays exponentially. Downstream the asymptote $-\bar{A} \sim \bar{X}^{0.4305}$ is attained. What is of interest here is that the flow separates on a shortened $O(Re\,\alpha^{-3})$ lengthscale and that the near-parabolic shape of the free surface is close in form to a hydraulic jump. These equations are also relevant to fully developed flow on a horizontal surface at large Fr (BS). This connection is to be expected since, from (2.3), $Fr \propto \alpha$ and for these large values of α the flow reacts so rapidly that the relatively shallow slope has little effect. However, we can include the effect of the sloping surface and the prescribed pressure gradient by altering the $P-A$ law (3.1g) to

$$\bar{P} = -\bar{A} - \bar{X}3^2\alpha^{-1}\lambda^{-3}, \quad \alpha \gg 1. \tag{3.2}$$

Now, far downstream $-\bar{A} \sim \bar{X}^{0.4305}$ so that the two terms in this law become comparable if $\bar{X} \sim O(\alpha^{1.7559})$. Further downstream it seems likely that the prescribed term in the law dominates and $\bar{A}$ attains the limiting form $\bar{A} \sim \bar{X}3^2\alpha^{-1}\lambda^{-3}$ with $\bar{P} \sim O(1)$. This, interpreted in terms of the original variables, $\hat{x}$ and $\hat{\eta}$, corresponds to a horizontal free surface with $\hat{\eta} = \alpha^*\hat{x}$ to first order.

When α increases to $O(Re^{2/7})$, we must include the effects of the cross-stream pressure gradient. The equations governing the development in this case have been found by Gajjar (1987) and we refer the reader there for the details of their derivation (see also BS). This follows similar lines to that of (3.1) and the scales of the interaction can be obtained by replacing α by $Re^{2/7}\tilde{\alpha}$. Nonlinear effects are felt when the free surface is displaced by an $O(Re^{-2/7})$ amount. The main part of the boundary layer is again relatively passive and the flow in the viscous sublayer is governed by (3.1) but with the $P-A$ law

$$\bar{P} = -d\tilde{\alpha}^7\bar{A}_{\bar{X}\bar{X}} - \bar{A}, \tag{3.3}$$

with $d = (2/5)\lambda^{10}3^{-6}$. This includes the extra contribution to the pressure from the streamline curvature. Again we have neglected, for the moment, the relatively small effect of the driving pressure gradient due to the slope.

Solutions of this set of equations for a free interaction are described in BS. These show the flow separating downstream with the asymptote $-\bar{A} \sim \bar{X}^{0.4305}$ being attained as on the smaller slopes discussed above. In addition, however, there is the possibility of oscillations in the free surface downstream caused by the interplay between the two inviscid terms on the right-hand side of (3.3). These are shown by BS to exist downstream of a small obstacle which causes linear perturbations to the basic shear profile. Gajjar (1987) also find them in linear and nonlinear flows over a convex corner. Large-amplitude disturbances with separation may be related to the wave hydraulic jump and the so-called surface shear wave described by Peregrine (1974), and de Silva & Peregrine (1988), although nonlinear free interactions with this pressure-displacement law in BS show no such oscillations. We emphasize that the full problem should take into account the downstream boundary conditions.

For slopes larger than $O(Re^{-5/7})$ the cross-stream pressure term dominates and the $P-A$ law becomes $\bar{P} = -d\tilde{\alpha}^7\bar{A}_{\bar{X}\bar{X}}$. This $P-A$ law has been studied by, for example, Smith (1976), Smith & Duck (1977) and Merkin & Smith (1982). The work of these authors indicates that there is a downstream form with separated flow and $\bar{A} \sim -\bar{P}_0\tilde{\alpha}^{-5}\bar{X}^2/2$ for $P_0 > 0$ and independent of $\tilde{\alpha}$ as $\bar{X} \to \infty$. This would correspond to separation of the liquid layer with the free surface remaining concave upwards, in contrast to the shape of the free surface on the smaller slopes discussed above. However, using an argument similar to that used by BS, the neglected gravitational term may be reinstated at large values of $\bar{X}$, as $\bar{A}$ becomes large but $\bar{A}_{\bar{X}\bar{X}}$ remains finite so that a jump with a blunt free surface may be seen. Which of these occurs depends

upon the influence of the prescribed pressure gradient due to the slope. Including these modifies the $P-A$ law to

$$\bar{P} = -d\tilde{\alpha}^7 \bar{A}_{\bar{X}\bar{X}} - \bar{A} + Re^{-2/7} 3^2 \lambda^{-3} \tilde{\alpha}^{-1} \bar{X}. \tag{3.4}$$

If we consider (3.4), as $\tilde{\alpha}$ and $\bar{X}$ becomes large, together with the result that downstream $\bar{A} = O(\tilde{\alpha}^{-5}\bar{X}^2)$, we see that the second term will only enter and give the blunt shape of the free surface if the distance required for it to become important, $\bar{X} \sim O(\tilde{\alpha}^{7/2})$, is sufficiently short. The last term, which causes the free surface to become horizontal, will enter and stop this occurring, when $\bar{X} \sim O(\tilde{\alpha}^3 Re^{2/7})$. So, for there to exist a region in which the free surface is convex upwards, we require $\tilde{\alpha}^{7/2} \ll \tilde{\alpha}^3 Re^{2/7}$, i.e. $\tilde{\alpha} \ll Re^{4/7}$ or $\alpha^* \ll Re^{-1/7}$. If this is not the case, as is true for slopes of $O(1)$ as $Re \to \infty$, the flow will not be affected at all by the gravitational term, $-\bar{A}$, in the pressure law. As a result the flow will proceed to attain a horizontal free surface with the free surface remaining concave throughout the interaction.

The other possibility we consider here is that of a train of waves after the jump. For small values of $\tilde{\alpha}$ the predominant balance is between the two terms on the right of (3.3) and the wavelength of the waves is $\bar{X} \sim \tilde{\alpha}^{7/2}$, i.e. $\hat{x} \sim O(Re^{1/7}\tilde{\alpha}^{1/2})$ or $O(Fr^{1/2})$. These shortened scales ensure the dominance of this inviscid balance. These are nothing other than long inviscid gravity waves on an ambient shear flow and able to stand on the stream, despite the large Froude number, since the flow is subcritical close to the bed. They suffer attenuation over the longer scale $\hat{x} \sim O(Re^{1/7}\tilde{\alpha}^{1/3})$ due to interaction with the wall layer. As $\tilde{\alpha}$ increases the wavelength increases to $O(Re^{1/7})$ and the waves become affected by a viscous–inviscid interaction at first order. Further downstream we would expect the prescribed term in the $P-A$ law to cause the free surface to become horizontal.

What form of the jump actually occurs is likely to depend crucially on the downstream boundary conditions and the flow within the separated region. A study of these effects is required to confirm the above prediction $\alpha^* \sim Re^{-1/7}$ for the change in the shape of the jump since, for a slope of only $O(Re^{-3/7})$, the crossover between the dominance of the effects of streamline curvature and those of gravity occurs after the free surface has moved an $O(1)$ distance and the separation becomes massive, in the sense that the displacement of the free surface can no longer be considered small as is required for (3.1) to hold. However, this study will not be carried out here.

Surface-tension effects, as can be seen from (2.2*b*), will result in the addition of a term $+\bar{A}_{\bar{X}\bar{X}}$ to the pressure-displacement law as noted by Gajjar (1987). If the coefficient of surface tension is large enough the initial departure will be wave-like. See Appendix B and BS who describe many of the novel properties of the interaction if surface tension dominates over streamline curvature. It is interesting to note also that the effects of surface tension can reduce the magnitude of the coefficient of the curvature term in (3.4) and allow the second, gravitational, term to enter before the growth of the last, prescribed, term destroys the interaction. Thus a large surface-tension coefficient ($B \sim O(Re^{2/7})$) will mean that such free interactions will be more likely to be seen as the slope increases.

4. The downstream form of the free interactions on slopes of $O(Re^{-1})$

4.1. *The governing equations*

On slopes of $O(Re^{-1})$ viscosity acts across the whole of the layer over the lengthscales upon which the self-induced pressure gradient is comparable with the prescribed pressure gradient due to the slope. Its effects are not confined to a sublayer at the bed

and the multistructured descriptions of §3 are not valid. The governing equations, derived by considering (2.1) and (2.2) in the limit $Re \to \infty$ with the scalings $\sin\alpha^* = Re^{-1}\alpha$, $\hat{x} = Re\,x$, $\hat{U} = U$, $\hat{V} = Re^{-1}(V + s'(x)\,U)$, and writing the reduced pressure $\hat{P} = \alpha x + Fr\,p$, $\hat{\eta} = \eta + \alpha x$ and $\hat{y} = y + s(x)$, are

$$U U_x + V U_y = -p_x + U_{yy}, \quad p_y = 0, \quad U_x + V_y = 0, \tag{4.1 a–c}$$

$$U = V = 0 \quad \text{at} \quad y = 0, \tag{4.1 d, e}$$

$$U_y = 0 \quad \text{at} \quad y = h(x) = 1 + \eta + \alpha x - s(x), \quad p = Fr^{-1}\eta, \tag{4.1 f, g}$$

with

$$\eta \sim -\alpha x \quad \text{as} \quad x \to \pm\infty. \tag{4.1 h}$$

The depth of the liquid layer is h and y measures distance normal to the bed. The conservation of mass flux implies

$$\int_0^h U(y)\,\mathrm{d}y = 1. \tag{4.1 i}$$

We can define a stream function $\psi(x, y)$ where $\psi_y = U$. We also have the relation $Fr^{-1}\alpha = 3$ from (2.3). The slopes which make up the obstacle $s(x)$ must be $O(Re^{-1})$.

4.2. *The numerical solution and the asymptote for the 'smaller' gradients*

In (4.1) we first set s identically equal to zero and omit the downstream boundary condition to study the free interaction. We seek solutions which illustrate the subsequent nonlinear development of the eigensolutions described in §2. We seed these eigensolutions by setting the initial depth to $1 + \delta$ with δ small, then march the solution forward in x. The numerical method, and in particular the technique used to deal with the unknown position of the free surface, is described in Appendix A. The solutions for a range of values of α and various initial perturbations are presented in figures 3 and 4.

One possible type of solution terminates in a so-called expansive singularity with the derivative of the layer's depth becoming large and negative and the skin friction becoming large and positive, although the depth of the layer remains of $O(1)$. The scales of the interaction shorten as this singularity is approached and we expect the prescribed pressure gradient due to the slope to become unimportant. There are two alternative forms of this singularity. The first (Bowles 1990) is akin to the structure of the expansive singularity in the closely related, problem of the free interaction in hypersonic flow (which is governed by (3.1) see Brown *et al.* 1974). This has

$$p_x \sim -P_s(x_0 - x)^{-3/5}(-\ln(x_0 - x))^{4/5} L_1(x_0 - x)$$

and

$$U_y(0) \sim T_s(x_0 - x)^{-3/5}(-\ln(x_0 - x))^{3/5} L_2(x_0 - x)$$

where P_s and T_s are unknown positive constants, the singularity occurs at $x = x_0$, and L_1 and L_2 are functions that vary more slowly than any power of a logarithm. The second structure (Higuera 1994) insists that the flow is critical, in the sense that waves on the velocity profile at the singularity cannot travel upstream, and gives the prediction $p_x \sim (x_0 - x)^{-0.69}$. See also Daniels (1992). A careful analysis, not presented here, of these computations shows that this second singularity is attained.

Another possible solution, illustrated in figure 3, has the free surface becoming horizontal. We note four points. First, for the case $\alpha = 0.25$, the approach to this

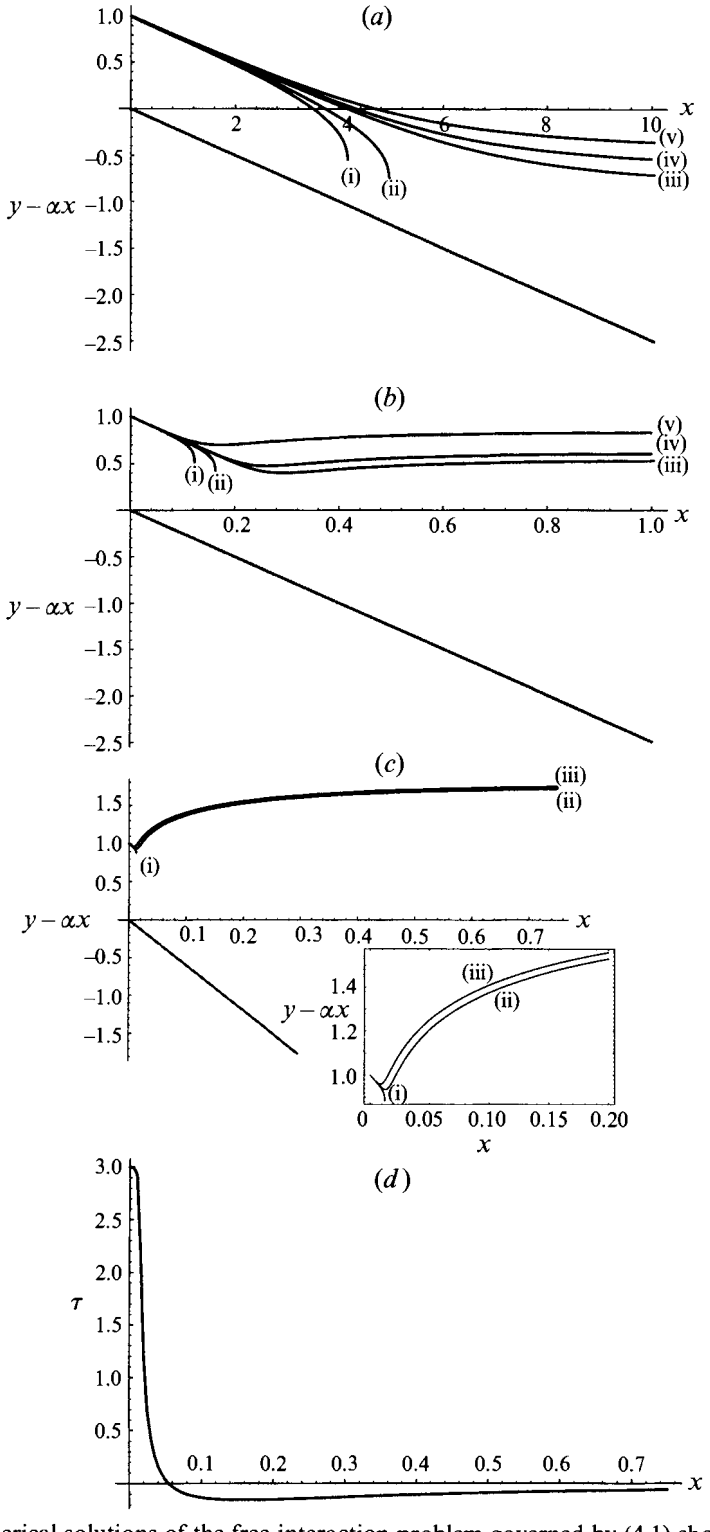

FIGURE 3. Numerical solutions of the free-interaction problem governed by (4.1) showing expansive interactions and the different forms of the compressive interactions on different slopes, α. In (*a–c*) the vertical axis is $y-\alpha x$, so that the lower, straight, line represents the bed. The other curves are the free

horizontal asymptote is from above, whilst for $\alpha = 2.5$ it is from below so that there is a region in which the free surface is convex upwards. Secondly, the flow exhibits self-induced separation for the larger slopes on these scalings, but not for the smaller slopes. Thirdly, the development lengthscale decreases as α increases in agreement with the predictions of §2. Fourthly, for the case $\alpha = 6$ the development is rapid and the blunt, near-parabolic, shape of the free surface supports the proposition in §2.2 that the limiting structure describing the development of the flow for large values of α is exactly that described in BS.

We now search for a description of the downstream form of these solutions. At the horizontal free surface far downstream we have the constraint $U_y = 0$. We therefore expect the flow far downstream to be Jeffrey–Hamel outflow through a diverging channel of angle $2\alpha^*$, if we restrict our attention to solutions which are symmetric about the midpoint of the channel (Jeffrey 1915; Hamel 1916; Rosenhead 1940; Fraenkel 1962). This relation between Jeffrey–Hamel flows and liquid-layer flows has been utilized by Eagles (1988) and PST, together with the assumption that the flow varies slowly and so maintains its Jeffrey–Hamel form, to study the development of liquid-layer flows over slowly varying obstacles and gradual changes in slope. In this work we are also concerned with more rapidly varying flows. Here we need consider only the high Reynolds number limit of Jeffrey–Hamel flows, with the angle between the plates $O(Re^{-1})$ as $Re \to \infty$.

At large values of x we have the scalings $y \sim x$, $U \sim 1/x$ from flux conservation, so that $p \sim U^2 \sim 1/x^2$. We write the position of the free surface as

$$y = 1 + \alpha x + Fr(p_0 + p_1/x^2 + \ldots), \quad x \to \infty \tag{4.2a}$$

and introduce the new variable

$$\xi = y/(1 + p_0 Fr + \alpha x). \tag{4.2b}$$

The value of p_0 will not be found in this large-x analysis. It is related to the total drop or rise in the free surface during the interaction and contains information about the history of the flow. Substitution into (4.1) yields, at $O(x^{-3})$, as $x \to \infty$,

$$\psi''' + \alpha\psi'^2 + 2p_1\alpha^3 = 0, \tag{4.3a}$$

$$\psi(1) = 1, \quad \psi''(1) = 0, \quad \psi(0) = \psi'(0) = 0, \tag{4.3b–e}$$

for the stream function ψ where $U = \psi'/x$ to first order and p_1 is to be found. Here the prime indicates $\partial/\partial\xi$. We make the substitutions $S = \alpha\psi'$, $\Lambda = 2\alpha^4 p_1$ and find

$$S'' + S^2 + \Lambda = 0, \tag{4.4a}$$

$$S'(1) = S(0) = 0, \quad \int_0^1 S\,\mathrm{d}\xi = \alpha. \tag{4.4b–d}$$

---

surface $y = 1 + \eta$ for different values of δ, the initial perturbation to the layer depth. Δx is the step length used in x and m is the number of points used in ξ (see Appendix A). (*a*) $\alpha = 0.25$, $\Delta x = 10^{-3}$, $m = 201$, $\delta = -5 \times 10^{-2}$, -2.5×10^{-2}, 1.25×10^{-2}, 2.5×10^{-2}, 5×10^{-2}, for the curves (i)–(v) respectively. The approach to the downstream asymptote is from above. Separation does not occur. (*b*) $\alpha = 2.5$, $\Delta x = 10^{-5}$, $m = 801$ for $\delta = 10^{-5}$, curve (iii), but $\Delta x = 10^{-3}$, $m = 201$, for $\delta = -10^{-3}$, -10^{-4}, 10^{-4}, 10^{-3}, curves (i), (ii), (iv), (v) respectively. The approach is now from below. (*c*) $\alpha = 6$, $\Delta x = 10^{-5}$, $m = 801$, $\delta = -10^{-6}$, 10^{-6}, 10^{-5} for curves (i)–(iii) respectively. The interaction develops rapidly and there is an obvious jump in the free-surface position. The inset shows the initial stages of the solutions more clearly. Separation occurs. (*d*) The development of the skin friction, $\tau = U_y$ at the bed, for the compressive solution shown in curve (iii) in (*c*) above.

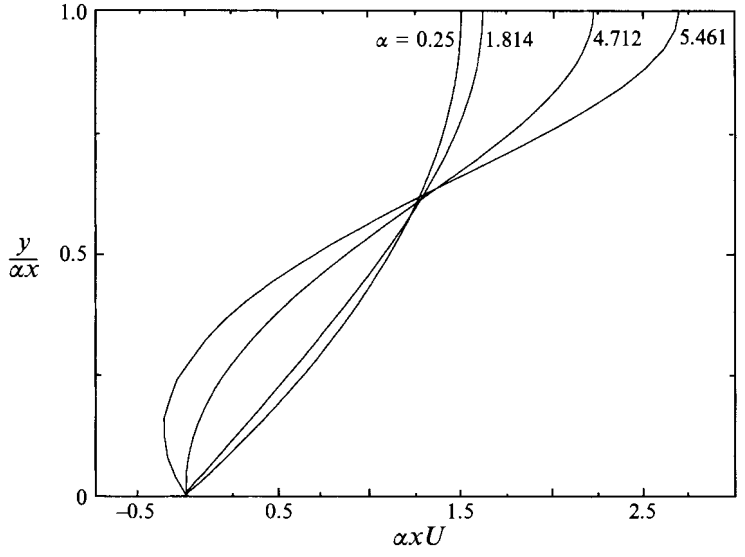

FIGURE 4. Typical downstream velocity profiles for the compressive interactions on different slopes ((i)–(v), $\alpha = 0.25, 1.814, 4.712, 5.461$). See the text and caption to figure 3.

This system can be solved in terms of elliptic functions. We summarize the results and draw attention to points of interest. For more details see Fraenkel (1962) or Eagles (1988).

For $\alpha < 2.998$ approximately there is a family of solution in which the skin friction at the bed is positive and $U'(y)$ is monotonically increasing. If Λ is positive the approach to the horizontal asymptote for the free surface is from above, if negative, it is from below. Of particular interest is the limit $\alpha \to 0$. From (4.4d) we expect S to be small in this limit so the nonlinear term in (4.4a) is lost and the predominant balance is between pressure and viscosity as in lubrication theory. Therefore the downstream form is one of half-Poiseuille flow, of linearly increasing depth. As Λ is $O(1)$, p_1 is large and the approach to this asymptote as x increases is slow.

A second slope of interest, covered by this type of solution, is that for which Λ changes sign. We consider (4.4) directly, putting $\Lambda = 0$. The solution has

$$\alpha = \frac{3}{2}\int_0^1 \frac{1}{(1-t^3)^{1/2}}\,\mathrm{d}t \int_0^1 \frac{t}{(1-t^3)^{1/2}}\,\mathrm{d}t = \frac{\pi}{3^{1/2}} \approx 1.814.$$

If α is bigger than this then the free interaction involves some range of x for which the free surface is convex upward.

For the range $2.998 < \alpha < 4.712$ approximately, U again increases monotonically from zero but there is a zero in U''. For $4.712 < \alpha < 5.461$ the velocity profiles exhibit regions of backflow close to the wall corresponding to separated flows. The case $\alpha = 4.712$ corresponds to a downstream asymptote with zero skin friction. For $\alpha > \alpha_c = 5.461$, there is no suitable Jeffrey–Hamel solution for net outflow, symmetric about the midpoint of a diverging channel. An alternative structure, involving a jet at the free surface, valid for all α but especially relevant to $\alpha > \alpha_c$, is described below.

The normalized velocity profiles in figure 4, calculated from (4.1), follow the pattern described above as α increases. The figure shows $\alpha x U$ far downstream, corresponding to $S(\xi)$. The curve for $\alpha = 0.25$ is very like a half-Poiseuille profile, whilst that for

$\alpha = 4.712$ exhibits zero skin friction, $U_y(0)$, as we predict. Theoretical values of the normalized free-surface velocity, $S(1)$ are 1.5, 1.625 and 2.18 for α equal to 0, 1.814 and 4.712 respectively and these predictions agree well with the calculations shown in the figure. In contrast, similar curves for larger values of α (not shown) exhibit separated flow but the product $\alpha x U$ does not asymptote to a constant profile as x increases. We conclude that an alternative asymptotic structure is relevant for these slopes and we believe this structure to be that described below.

4.3. *An alternative flow structure for large x; breakaway separation*

An alternative form for the downstream asymptote has the vorticity breaking away from the wall to form a jet at the free surface, instead of being distributed across the depth of the layer by viscous action as in Jeffrey–Hamel flow. Beneath this jet, which contains the majority of the downstream mass flux and momentum flux of the flow, is an irrotational region of backflow and a reversed-flow boundary layer at the wall. This 'breakaway separation' can be expected to occur for the larger values of α since for these slopes the development is too rapid for viscosity to redistribute vorticity across the layer. This flow may also be considered as the ultimate form of the downstream development of the separated flows beneath a free surface described in §3, as the influence of viscosity is felt across the depth of the layer on an $O(Re)$ lengthscale.

Consider (4.1) in the limit of large x with flow beneath a horizontal free surface. The thickness of the layer is given by $\alpha x + p\,Fr$, where p is the pressure. Without loss of generality we can ignore the $O(1)$ contribution to the pressure and so free-surface position, effectively fixing the origin of the x-coordinate. The flow divides into three regions. See figure 5. Region I, near to the free surface, is of thickness $O(x^{2/3})$ and here we use the variable $\chi = (\alpha x + p\,Fr - y)/x^{2/3}$, so $\chi = 0$ at the free surface and approaches infinity towards the interior. The stream function, ψ, is $O(x^{1/3})$, and the velocity profile here turns out to be that of a $\mathrm{sech}^2\chi$-like jet, with the velocities $O(x^{-1/3})$ so that the jet slows as it spreads. In the main part of the flow, region II, which is of thickness $O(x)$, there is a slow backflow with $\psi \sim O(x^{1/3})$ and $U \sim O(x^{-2/3})$. The flow here is inviscid and irrotational. Viscosity reduces the slip velocity to zero in region III, a reversed-flow boundary layer at the lower wall of thickness Δ say. To ensure that viscous and inertial terms (of sizes $U^2/x \sim O(x^{-7/3})$ and $U/\Delta^2 \sim x^{-2/3}/\Delta^2$ respectively) balance, requires $\Delta \sim O(x^{5/6})$ so that $\psi \sim O(x^{1/6})$. We combine regions II and III in the analysis below and use the variable $\zeta = y/x^{5/6}$ to describe it. This is possible because region II is described by the large-ζ (inviscid) limit of the equations of region III. The variables ζ and χ are related by

$$\zeta = \alpha x^{1/6} - x^{-1/6}\chi + Fr\,p x^{-5/6}. \tag{4.5}$$

With this structure, then, we expand as follows. In region I,

$$\psi \sim -(x^{1/3} f_1(\chi) + x^{1/6} f_2(\chi) + f_3(\chi) + \ldots). \tag{4.6}$$

In region III,

$$\psi \sim x^{1/6} g_1(\zeta) + g_2(\zeta) + x^{-1/6} g_3(\zeta) + \ldots, \tag{4.7a}$$

and

$$p \sim -(p_1 x^{-4/3} + p_2 x^{-3/2} + p_3 x^{-5/3} + \ldots). \tag{4.7b}$$

The relevant boundary conditions are $f_i''(0) = f_i(0) = 0$, as the change in position of the free surface has yet to have an effect, with the exception that $f_3(0) = -1$ for the net mass flux to be unity. The value of $f_1'(\infty)$ should be zero to match with the slow reversed flow in region II. The other $f_i(\infty)$ should be match with the higher-order solutions in region II. Here, $g_i(0) = g_i'(0) = 0$ and $g_i'(\infty) < 0$ to give reversed flow in the main body of the layer.

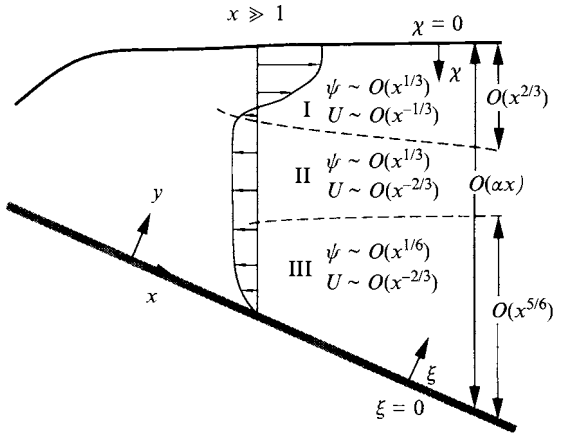

FIGURE 5. The structure of the flow at large distances after breakaway separation showing the coordinate system used and the regions I–III referred to in §4.3.

Substituting the above asymptotes into (4.1) and using the result, derived below, that f_2 turns out to be zero in the equation for f_3 gives the following:

$$f_1''' + \tfrac{1}{3}(f_1 f_1'' + f_1'^2) = 0, \tag{4.8a}$$

$$f_2''' + \tfrac{1}{3} f_1 f_2'' + \tfrac{5}{6} f_1' f_2' + \tfrac{1}{6} f_1'' f_2 = 0, \tag{4.8b}$$

$$f_3''' + \tfrac{1}{3} f_1 f_3'' + f_1' f_3' = 0, \tag{4.8c}$$

where the prime indicates $\partial/\partial\chi$. Also,

$$g_1''' + \tfrac{1}{6} g_1 g_1'' + \tfrac{2}{3}(g_1'^2 - 2p_1) = 0, \tag{4.9a}$$

$$g_2''' + \tfrac{1}{6} g_1 g_2'' + \tfrac{3}{2}(g_1' g_2' - p_2) = 0, \tag{4.9b}$$

$$g_3''' + \tfrac{1}{6} g_1 g_3'' - \tfrac{1}{6} g_1'' g_3 + \tfrac{5}{3}(g_1' g_3' - p_3 + \tfrac{1}{2} g_2'^2) = 0, \tag{4.9c}$$

where the prime indicates $\partial/\partial\xi$. We note that in the main part of the flow, region II, where the vorticity is zero, these equations give p_1 to p_3 in terms of the backflow velocities $g_i'(\infty)$.

In region I, f_1 is found to be

$$f_1(\chi) = a \tanh(a\chi/6), \tag{4.10}$$

where a is an arbitrary constant. This gives a jet with a velocity $\propto \operatorname{sech}^2(a\chi/6)$ near the free surface. The value of a is undetermined. The momentum flux contained within the jet is $a^3/9$, and is $O(1)$ as $x \to \infty$. The pressure is asymptotically zero as the free surface is horizontal and the shear stresses at the free surface and at the wall are zero and $O(x^{-3/2})$ respectively. An application of the momentum integral theorem, therefore, suggests that this momentum flux is the same as that emerging from the interaction at $x \sim O(1)$, and so is equal to that of the original profile except for some possible losses in the process of separation. These losses are due to either viscous stresses at the wall or work done by the initial flow in countering any rise in depth and so adverse pressure gradient, near to the start of the interaction.

Since $f_i = f_1'$ is a complementary function to all the equations for f_i, $i \geqslant 2$, we may write the full complementary function for f_i, $i \geqslant 2$, in the form

$$f_i = C_i \operatorname{sech}^2 z - \tfrac{1}{2} \operatorname{sech}^2 z \int_1^{\operatorname{sech}^2 z} \frac{\mathscr{H}_i(u)}{u^2(1-u)^{1/2}}\,\mathrm{d}u, \tag{4.11}$$

where here $z = a\chi/6$ and $\mathscr{H}_i(u) = A_i F(r,s;1;u) + B_i F(r,s;\frac{1}{2};1-u) = A_i\phi_1 + B_i\phi_2$ say. Here F is the hypergeometric function (Abramowitz & Stegun 1965), with $r+s = 1/2$ and $rs = (1-i)/4$. Using the asymptotic forms of ϕ_1 and ϕ_2 we are led to the following relationships between the unknown constants:

$$f_i \sim B_i \frac{\Gamma(\frac{1}{2})}{\Gamma(r)\Gamma(s)} z + \frac{1}{2}\left(A_i + B_i \frac{\Gamma(\frac{1}{2})(K_0 - 1 - \ln 4)}{\Gamma(r)\Gamma(s)}\right) \quad \text{as} \quad z \to \infty, \tag{4.12a}$$

$$f_i(0) = C_i, \quad f_{iz}(0) = A_i \frac{\Gamma(\frac{1}{2})}{\Gamma(1-r)\Gamma(1-s)} + B_i, \quad f_{izz}(0) = -2C_i + A_i \frac{\Gamma(-\frac{1}{2})}{\Gamma(r)\Gamma(s)}, \tag{4.12b–d}$$

where $K_0 = 2\psi(1) - \psi(r) - \psi(s)$, with ψ here representing the di-gamma function, Γ'/Γ. Hence, using the boundary conditions, we find $C_2 = A_2 = 0$, $C_3 = -1$, and $A_3 = -2$.

The equations in region II, for the reversed flow, must be solved numerically.

The transformations

$$\hat{\zeta} = \zeta \frac{(2p_1)^{1/4}}{\sqrt{6}}, \quad \sigma = p_3 - \frac{p_2^2}{4p_1}, \quad \mu = \frac{p_2^2}{4p_1\sigma}, \tag{4.13a–c}$$

$$\gamma_1 = \sqrt{6}(2p_1)^{1/4}, \quad \gamma_2 = \sqrt{6}\frac{p_2}{(2p_1)^{3/4}}, \quad \gamma_3 = \frac{\sigma\sqrt{6}}{(2p_1)^{3/4}}, \tag{4.13d–f}$$

$$g_i = \gamma_i \hat{g}_i(\hat{\zeta}), \tag{4.13g}$$

lead to the normalized equations

$$\hat{g}_1''' + \hat{g}_1\hat{g}_1'' + 4(\hat{g}_1'^2 - 1) = 0, \quad \hat{g}_2''' + \hat{g}_2''\hat{g}_1 + 9(\hat{g}_1'\hat{g}_2' - 1) = 0, \tag{4.14a, b}$$

$$\hat{g}_3''' + \hat{g}_3''\hat{g}_1 - \hat{g}_3\hat{g}_1'' + 10(\hat{g}_1'\hat{g}_3' - 1 + \mu(\hat{g}_2'^2 - 1)) = 0, \tag{4.14c}$$

with boundary conditions $\hat{g}_i(0) = \hat{g}_i'(0) = 0$, $\hat{g}_i \sim -\hat{\zeta} + \hat{c}_i$ at infinity to ensure irrotational flow in region II. The $\hat{c}_i$ are constants to be found numerically. We solve (4.14) using finite-difference methods and check the results using a variety of grid sizes and ranges of integration. We find $\hat{g}_1''(0) = -2.273$, $\hat{c}_1 = 0.414$, $\hat{g}_2''(0) = -3.715$, $\hat{c}_2 = -0.140$. The constant $\hat{c}_3$ depends on μ, which turns out to be independent of a but not of α, and therefore no unique value can be given to it. The decay toward the reversed-flow solutions at infinity is like $\hat{\zeta}^{-7}$, i.e. algebraic.

We may match the solutions in regions I and II, to find the unknown coefficients and the pressure. Writing $c_i = \hat{\gamma}_i \hat{c}_i$ and using (4.5) to write the solution in region II as $\zeta \to \infty$ in terms of χ, we find

$$\psi \sim x^{1/3}(-\alpha(2p_1)^{1/2}) + x^{1/6}\left(c_1 - \frac{\alpha p_2}{(2p_1)^{1/2}}\right) + \left((2p_1)^{1/2}\chi + c_2 - \frac{\sigma}{(2p_1)^{1/2}}\right) \quad \text{as} \quad \zeta \to \infty. \tag{4.15}$$

So, matching, we find, from the $O(x^{1/3})$ term, $p_1 = (a/\alpha)^2/2$ since $f_1(\infty) = a$. At $O(x^{1/6})$ there are no terms proportional to χ in (4.15) and therefore $B_2 = 0$ from (4.12a). Since then A_2 and C_2 are also zero, from (4.12b) and (4.12c), we find $f_2 = 0$ and $p_2 = c_1(2p_1)^{1/2}/\alpha = 1.014a^{3/2}\alpha^{-5/2}$. At $O(1)$ we get, using (4.12a) with $r = 1$, $s = -1/2$, $B_3 = -12/\alpha$, $\sigma = -a(1 + 9.348/\alpha)/\alpha^2$ and

$$f_3(\chi) = -1 + \frac{a\chi}{\alpha} - \frac{9}{\alpha}\left(\frac{a\chi}{6}\operatorname{sech}^2\frac{a\chi}{6} + \tanh\frac{a\chi}{6}\right), \tag{4.16}$$

using a relationship between hypergeometric functions and Legendre polynomials.

In principle higher-order terms in this expansion can be found. There is new physics entering at $O(x^{-2/3})$, due to the change in the position of the free surface, and at $O(x^{-1})$ due to the algebraic decay of the solutions in region III. Uncertainties over the $O(1)$ position of the free surface, i.e. the pressure rise in separation, and the origin of the expansion in x, would bring in eigensolutions to the problem but these have been suppressed as mentioned above. None of these extra effects, however, serve to fix the value of a which depends on the momentum flux emerging from the region $x = O(1)$. In summary, therefore, given both a and α,

$$p \sim -\left(\frac{a^2}{2\alpha^2}x^{-4/3} + 1.014\frac{a^{3/2}}{\alpha^{5/2}}x^{-3/2} - \left(\frac{a}{\alpha^2} + 8.834\frac{a}{\alpha^3}\right)x^{-5/3} + \ldots\right), \tag{4.17a}$$

$$U_y(0) \sim -0.928\frac{a^{3/2}}{\alpha^{3/2}}x^{-3/2}\left(1 + 1.657\frac{x^{-1/6}}{a} + \ldots\right). \tag{4.17b}$$

The momentum flux of the oncoming flow, except for any losses at separation, is concentrated into a free jet near to the free surface. The speed of this jet is $O(x^{-1/3})$, which is faster than the $O(x^{-1})$ velocities in the Jeffrey–Hamel flow of §4.2. The large volume flux in the jet is balanced by a slower backflow in the wider main part of the thickening layer which is brought to zero by a boundary layer at the wall. The pressure gradient is simply that required to drive the backflow which, at higher orders, is also affected by the boundary layer's displacement. It seems possible to accommodate any momentum flux and therefore any oncoming-flow/separation pair with a structure of this kind. It is worth noting that this structure, at least to these lower orders, before the position of the free surface enters into the expansion, can describe the asymptotic form of breakaway separation in a diverging channel. The differences appearing at higher orders will not result in the general form of the expansion becoming unsuitable.

5. The limit of small gradient

5.1. *The governing equation*

We have seen in §§2.2 and 4.2 that, if the scaled slope, α, is small, the flow remains of half-Poiseuille type throughout the compressive free interaction. Both the initial stages and the final large-$\hat{x}$ asymptote, with a horizontal free surface, are governed by lubrication theory. The development in $\hat{x}$ is slow and viscosity acts to redistribute the vorticity and keep the flow half-Poiseuille in character. This means that separation is not possible.

The lubrication approximation has been used by many authors to derive equations governing the behaviour of liquid films, specifically in this context by PST. We write the depth of the layer as $h(X)$ where $X = \hat{x}\sin\bar{\alpha}$ and in the limit $\sin\bar{\alpha} \to 0$, assuming $Re\sin\bar{\alpha} \ll 1$, the Navier–Stokes equations reduce to the ordinary differential equation

$$h_X - \gamma h_{XXX} = 1 - \frac{1}{h^3} - s_X + \gamma s_{XXX}, \tag{5.1}$$

where $\gamma = B\sin^2\bar{\alpha}$ and $s(X)$ describes any obstacle on the slope. The basic slope has been scaled to be unity. We refer the reader to PST for the details of the derivation. The equation remains a valid description of the flow as long as $h^3 \gg \sin\alpha^*$.

Here we investigate the solutions of (5.1) with $\gamma = 0$, in both forced and free interactions, using both analytical and numerical solutions. The free interaction in the

limit of large γ is considered in Appendix B. We aim, by a study of this reduced equation, to shed light on the structure of the forced interaction on larger slopes.

5.2. *Free and forced interactions on shallow slopes*

In this section we concentrate on the case $\gamma = 0$, so that

$$h_X = 1 - \frac{1}{h^3} - s_X, \quad h \to 1, \quad X \to \pm\infty. \tag{5.2a, b}$$

This equation contains within it the possibility of free interaction. If we consider the case $s = 0$ and neglect the boundary condition as $X \to \infty$ we see that a possible solution is $h = 1$. This is not unique and we have seen in §2.2 that an initially small disturbance of the form $h = 1 + \epsilon g(X)$, $\epsilon \ll 1$, will grow according to $g_X = 3g$ which implies $g = k\exp(3X)$ with k arbitrary. Further downstream we have the three possible asymptotes $h \sim X$, $h \sim 1$ or $h \sim (4(X_0 - X))^{1/4}$ for some finite X_0. The first of these ($k > 0$) corresponds to the compressive free interaction studied in §4.2. The second is undisturbed flow ($k = 0$) and the last ($k < 0$) will lead to the expansive interaction. As the layer thins inertial effects will become important. In the case of a large Reynolds number, the final form of this interaction will be governed by the full boundary-layer equations with the singularity described in §4.2 being attained.

We now turn to the forced interaction. The numerical solution of the forced interaction by marching forward from $X = -\infty$ is unstable and the solution attains either the first or the third of the three forms described above and not the downstream boundary condition. The numerical solution can be rendered stable by integrating from $+\infty$ imposing the boundary condition relevant there. (The author is grateful to Dr S. J. Tavener for drawing his attention to this fact.) All the numerical solutions presented in this section are obtained using this technique. We first consider a case which can be solved analytically and which exhibits many of the features common to forced interactions (see Smith 1982). The case considered is that of a simple change in slope at $X = 0$,

$$s_X = 0, \quad X < 0, \qquad s_X = \beta, \quad X \geqslant 0. \tag{5.3a, b}$$

A numerical solution of this problem, with $\beta = 4/5$ is presented in figure 6. In the limit $\beta \to 1-$ the slope downstream of $X = 0$ becomes nearly horizontal and the depth of the layer becomes large. As $\beta \to -\infty$, in contrast, the gradient increases and inertial effects must enter as the layer thins. For $X > 0$ (5.2*a*) reduces to

$$h_X = (1-\beta) - 1/h^3. \tag{5.4}$$

The appropriate downstream boundary condition is $h_X \to 0$ as $X \to \infty$, corresponding to uniform flow downstream. It is clear from the arguments presented above for the free interaction that the only possible solution has $h_X = 0$ for all positive X, i.e. $h = (1-\beta)^{-1/3}$ for $X > 0$. This implies that $h(0) = (1-\beta)^{-1/3}$ and so for $X < 0$ we have

$$h_X = 1 - 1/h^3, \quad h(0) = (1-\beta)^{-1/3}. \tag{5.5a, b}$$

If we write $(1-\beta)^{-1/3} = \delta$, then this equation has a solution given implicitly by

$$X = (h-\delta) + \tfrac{1}{3}\ln\left|\frac{h-1}{\delta-1}\left(\frac{\delta^2+\delta+1}{h^2+h+1}\right)^{1/2}\right| - \frac{1}{\sqrt{3}}\tan^{-1}\left(\frac{(2/\sqrt{3})(h-\delta)}{1+\frac{4}{3}(h+\frac{1}{2})(\delta+\frac{1}{2})}\right). \tag{5.6}$$

If we examine this as $\delta \to \infty$ ($\beta \to 1-$), corresponding to the downstream slope nearing the horizontal and so the depth there becoming infinite, we find, writing $\hat{h} = \delta h$

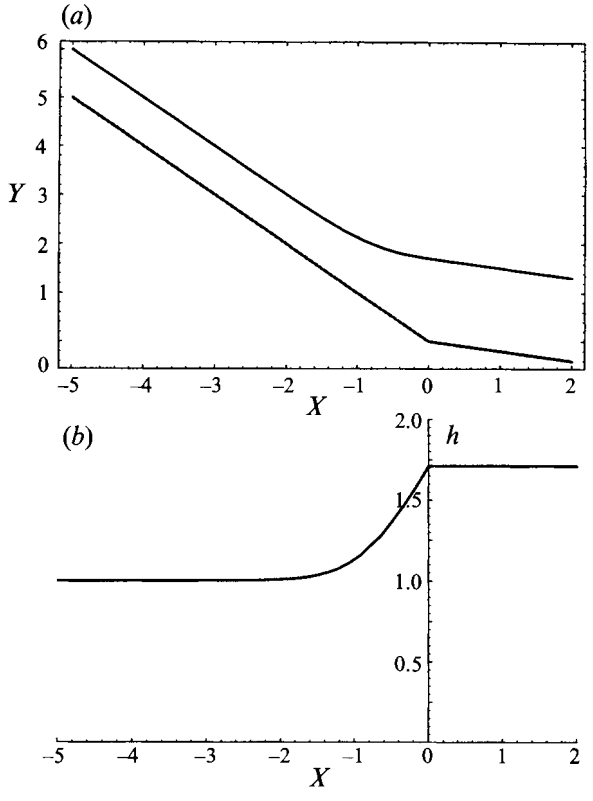

FIGURE 6. A numerical solution of (5.2) with s given by (5.3) with $\beta = 4/5$ corresponding to liquid-layer flow on a shallow slope encountering a decrease in the gradient. (*a*) The variation with X of the bed (the lower curve, $Y = -X + s(X)$) and the free-surface position (the upper curve, $Y = -X + s(X) + h$). (*b*) The depth $h(X)$.

and $\hat{X} = \delta X$, where $\hat{h}$ and $\hat{X}$ remain $O(1)$ as $\delta \to \infty$, that $\hat{h} \sim 1 + \hat{X}$. This implies that upstream of $X = 0$ the free surface is horizontal and the depth alters owing to the slope. In this vicinity of $\hat{X} = -1$, i.e. $X = -\delta$, the depth becomes $O(1)$ and the solution here is

$$X + \delta = h + \tfrac{1}{3}\ln\left|\frac{h-1}{(h^2+h+1)^{1/2}}\right| + \frac{1}{\sqrt{3}}\tan^{-1}\left(\frac{\sqrt{3}}{2h+1}\right). \tag{5.7}$$

This is the solution of (5.2*a*) for a compressive free interaction, i.e. $s = 0$ and $h = 1 + k\exp 3X$ far upstream with k positive. As $X + \delta \to -\infty$ the solution is

$$h = 1 + \sqrt{3}\exp(3(X+\delta)), \tag{5.8}$$

corresponding to the form of the solution predicted for the free interaction and giving k explicitly. For finite δ the solution is more complicated, but as $X \to -\infty$ it always has the form $h = 1 + k\exp(3X)$, where

$$k = (\delta - 1)\frac{\sqrt{3}}{(\delta^2+\delta+1)^{1/2}}\exp\left(3(\delta-1) + \sqrt{3}\tan^{-1}\left(\frac{1}{\sqrt{3}}\left(\frac{1-\delta}{1+\delta}\right)\right)\right). \tag{5.9}$$

If now $\delta \gg 1$ this reduces to $k \sim \sqrt{3}\exp(3\delta)$, and this agrees with the result (5.8), corresponding to the position of the free interaction moving a distance $O(\delta)$ upstream.

On the other hand, if we consider the case of a large increase in slope so that $\delta \to 0+$, then

$$k \sim -\frac{\sqrt{3}}{\delta}\exp\left(-3+\sqrt{3}\tan^{-1}\left(\frac{1}{\sqrt{3}}\right)\right), \tag{5.10}$$

and this indicates that the adjustment towards a large increase in slope starts at a position $O(-\ln(\delta))$ upstream. Of course the limit $\delta \to 0$ is not strictly valid as inertial effects will enter near $X = 0$ as the depth decreases. It seems likely, however, that the initial stages of the interaction will be governed by lubrication theory and this result will hold upstream of $X = 0$ as $\delta \to 0$.

This simple example has a complete analytical solution and illustrates features common to many forced interaction problems, in particular the movement of the start of the interaction upstream as the size of the departure from uniform flow increases. Also clear is the development, in the limit $\delta \to \infty$, of a flow containing a free interaction far upstream of $X = 0$.

5.3. *The asymptotic structure of flow over a large obstacle on a shallow slope*

Numerical solutions of (5.2) for a range of obstacles are illustrated in figure 7. The height of the free surface above some horizontal datum does not increase as the flow thickens, which may be proved by considering (5.2). The solution for flow over a single obstacle has an asymptotic structure as the height of the obstacle, d say, increases but with the width remaining $O(1)$, which we now describe. We write the governing equation as

$$h_X = 1 - \frac{1}{h^3} - ds_X, \tag{5.11a}$$

$$s = O(1) \quad \text{as} \quad d \to \infty, \quad h \to 1 \quad \text{as} \quad X \to \pm\infty, \tag{5.11b,c}$$

$$s \sim 1 - s_0 X^2/2 \quad \text{as} \quad X \to 0, \tag{5.11d}$$

where, in addition, $s(X)$ decays exponentially for large $|X|$. Here s_0 is the second derivative of the obstacle shape at the crest which is typically of the type used in the numerical solutions in figure 7. We presume too, that it is symmetric about $X = 0$ but this can easily be relaxed. We look for a solution of the type suggested by the numerical solutions and consider the equation in the following four regions. See figure 8.

First, on the lee side and on the slope downstream of the obstacle (region I), the primary balance is local in character and h_X is relatively small. The solution is $h \sim (1 - ds_X)^{-1/3}$, as $d \to \infty$. Thus as $X \to \infty$ and s decays exponentially to zero, $h \to 1$. The depth is determined solely by the local slope, so for this asymptotic structure to be valid, $\sin\alpha^* \ll d^{-1}$. As $X \to 0+$, i.e. approaching the crest of the obstacle, we find, for large d, that

$$h \sim (ds_0)^{-1/3}X^{-1/3} - \tfrac{1}{3}(ds_0)^{-4/3}X^{-4/3}(1 + O(X)), \tag{5.12}$$

since s is locally symmetric.

Secondly, near the crest of the obstacle (i.e. near $X = 0$, region II) the slope nears zero and so a locally defined depth would be infinite. To counter this the non-local term h_X enters and a balance including this effect is possible if $h \sim O(d^{-1/7})$ and $X \sim O(d^{-4/7})$. Therefore we write $h = \hat{h}d^{-1/7}$, $X = \xi d^{-4/7}$, with $\hat{h}$ and ξ both $O(1)$ as $d \to \infty$, and find

$$\hat{h}_\xi = -\frac{1}{\hat{h}^3} + \xi s_0 + \frac{1}{d^{3/7}} + O(d^{-4/7}) \tag{5.13}$$

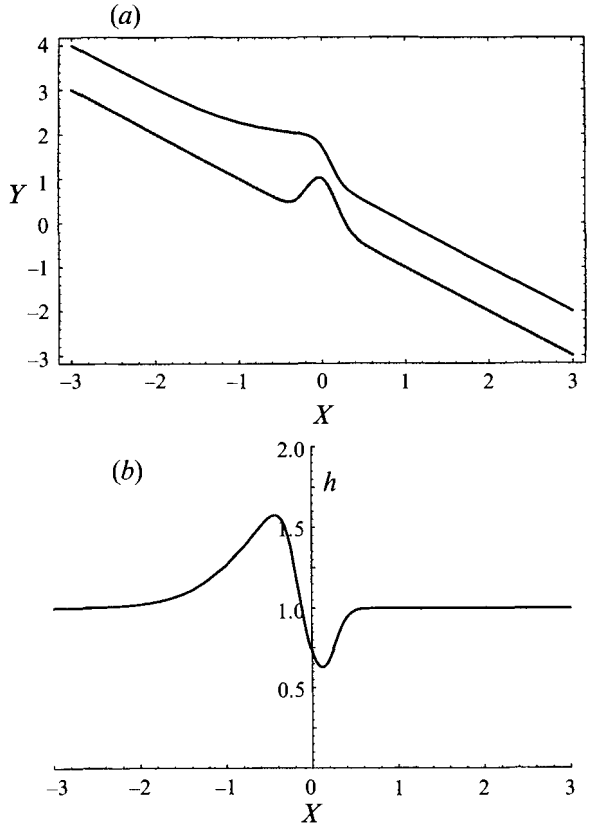

FIGURE 7(*a*, *b*). For caption see facing page.

as $d \to \infty$. We now write $\hat{h} = \hat{h}_0 + d^{-3/7}\hat{h}_1$, and substitute into (5.13) to get, with boundary conditions from (5.12),

$$\hat{h}_{0\xi} = -\frac{1}{\hat{h}_0^3} + \xi s_0, \quad \hat{h}_0 \sim (s_0\xi)^{-1/3} \quad \text{as} \quad \xi \to \infty, \tag{5.14a, b}$$

$$\hat{h}_{1\xi} = 3\frac{\hat{h}_1}{\hat{h}_0^4}, \quad \hat{h}_1 \sim -\tfrac{1}{3}(s_0\xi)^{-4/3} \quad \text{as} \quad \xi \to \infty. \tag{5.14c, d}$$

Equation (5.14*a*) can be solved numerically. This has not been done since it seems clear that a solution can be found by starting the integration at downstream infinity. The asymptotes as $\xi \to -\infty$ are

$$\hat{h}_0 \sim \frac{\xi^2 s_0}{2} + E_0 + \tfrac{8}{5}s_0^{-3}\xi^{-5} - \frac{48E_0}{7}s_0^{-4}\xi^{-7} + \ldots, \tag{5.15a}$$

and

$$\hat{h}_1 \sim \xi + E_1 + \ldots. \tag{5.15b}$$

The value of E_0 is fixed by (5.14*a*) and is of the form $E_0 = \tilde{e}s_0^{-1/7}$ for a number $\tilde{e}$ which is independent of the obstacle. E_1 is also fixed and can be calculated from the relation (5.14*c*).

Thirdly, upstream of the obstacle (region III), from (5.15) we see that, as $X \to 0-$, $h \sim dX^2/2 + X + d^{-1/7}E_0 + d^{-4/7}E_1 + \ldots$ and so we write, for $X < 0$,

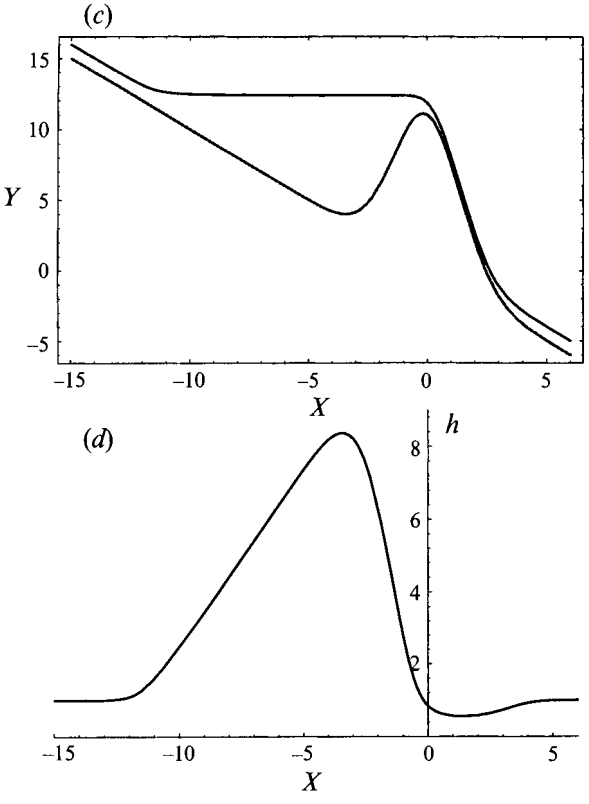

FIGURE 7. Numerical solutions of (5.2) with s given by $d\exp(-(X/b)^2)$. (a, c). The variation with X of the bed (the lower curve, $Y=-X+s(X)$) and the free-surface position (the upper curve, $Y=-X+s(X)+h$). (b, d) The depth $h(X)$. (a, b) $d=1$, $b=1/4$, (c, d) $d=11$, $b=2$.

$h = dH_0+H_1+d^{-1/7}H_2+d^{-4/7}H_3+\ldots$. Substitution of a solution of this form into (5.11) gives, on matching with (5.15), $H_0=1-s$, $H_1=X$, $H_2=E_1$, $H_3=E_1$, and as $X\to-\infty$ we find that

$$h\sim d+X+d^{-1/7}E_0+d^{-4/7}E_1+\ldots. \tag{5.16}$$

Lastly, we consider the region in the vicinity of $X=-d$ (region IV). Here h becomes $O(1)$ once more and we expect a free interaction to occur. To leading order the position of this interaction is $X=-d$, as found earlier in this section for the case of an adjustment of the flow to that on a nearly horizontal slope. However, in this case we have shown that the next term in the position of the interaction is $\tilde{e}_0(s_0 d)^{-1/7}$ and so depends on the curvature of the obstacle at its crest, with a sharper crest having a smaller effect on the upstream behaviour of the solution. If $X=-d-E_0 d^{-1/7}-E_1 d^{-4/7}+\zeta$ then in the vicinity of $\zeta=O(1)$, as $d\to\infty$, the flow is governed by the equation of the free interaction and this ensures that $h\to 1$ as $X\to-\infty$.

6. Forced interactions on larger slopes and comparison with experiments

6.1. *Forced interactions on slopes of* $O(Re^{-1})$

We present in figure 9 some solutions of (4.1) corresponding to a liquid adjusting to a change in slope or negotiating an obstacle placed on the slope. These are obtained using the numerical scheme described in Appendix C. Figure 9(*a*) shows the free

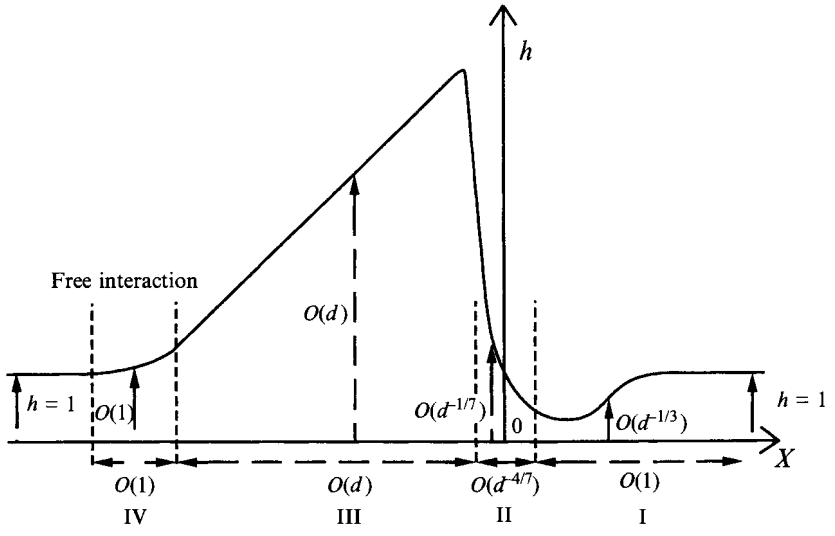

FIGURE 8. The asymptotic structure of the solution for the depth h of viscous liquid layer flow over a ridge of height $d \gg 1$ and of $O(1)$ width mounted on a shallow slope. The ridge is centred at $X = 0$. The regions I–IV referred to in §5.3 are illustrated.

surface and the bed for flow adjusting from an upstream slope $\alpha = \alpha_U = 5$ to a downstream slope $\alpha = \alpha_D = 0.2$. We take $s(x) = 0$ for $x < 0$ and $s(x) = (\alpha_D - \alpha_U)\, x \tanh bx$ for $x > 0$ with here $b = 2$. The depth and skin friction are sown in figure 9(b, c), together with results for $\alpha_U = 5$, $\alpha_D = 1$, $b = 1$. There is an obvious jump in the free-surface position. For the case $\alpha_D = 0.2$, for which the downstream depth is quite large ($h = 2.92$) this is on the upstream slope and is short-scaled, as predicted in §2.2, ($q \sim 526$ for $\alpha = 5$), and locally h_x is large. The free surface also has the blunt shape predicted in §3 and seen in the free-interaction calculations of §4.2 (for the case $\alpha = 6$). We would expect the jump to move further upstream as the downstream depth increased, as was seen in the lubrication solutions of §5.2. In the present case, however, owing to the larger Froude number, the adjustment is rapid and takes the form of a jump. The flow also separates within the jump and reattaches at some $x > 0$, presumably because of the influence of the bed there. For the case $\alpha_D = 1$, the downstream depth is smaller ($h = 1.7$) and the jump is seen to occur further downstream, in fact where $x > 0$ ($x \approx 0.3$) so that the local slope is much reduced. As a consequence the lengthscale of the jump is increased and the flow does not separate. The alteration in the depth and skin friction in the range $0 < x < 0.3$ is gradual and is due to the local change in slope. In these solutions then we see the emergence of two distinct scales for the flow. The long scale over which the flow adjusts gradually and the short scales of the hydraulic jump.

Figure 9$(d$–$f)$ shows the results of calculations corresponding to flow over a ridge, $s(x) = d\exp(-x^2/w^2)$ with $d = 20$, $w = 2$ and $d = 24$, $w = 3$. These show similar flow characteristics to the results described above.

6.2. *Comparison with experiments*

Experiments and computations of the full Navier–Stokes equations which cover approximately the range $\tan\alpha^* = O(Re^{-5/7})$ or less have been performed by PST. We now compare the predictions of the theory developed in this paper with the results of these experiments.

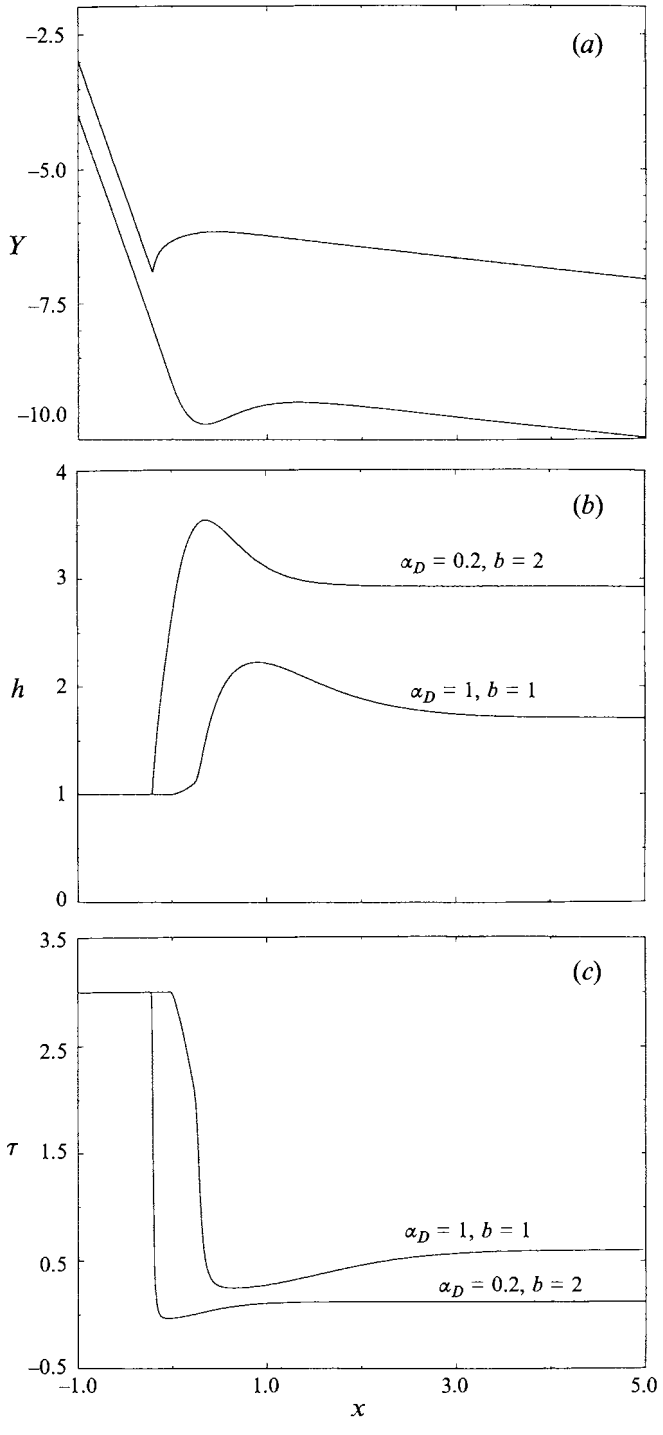

FIGURE 9(*a–c*). For caption see page 88.

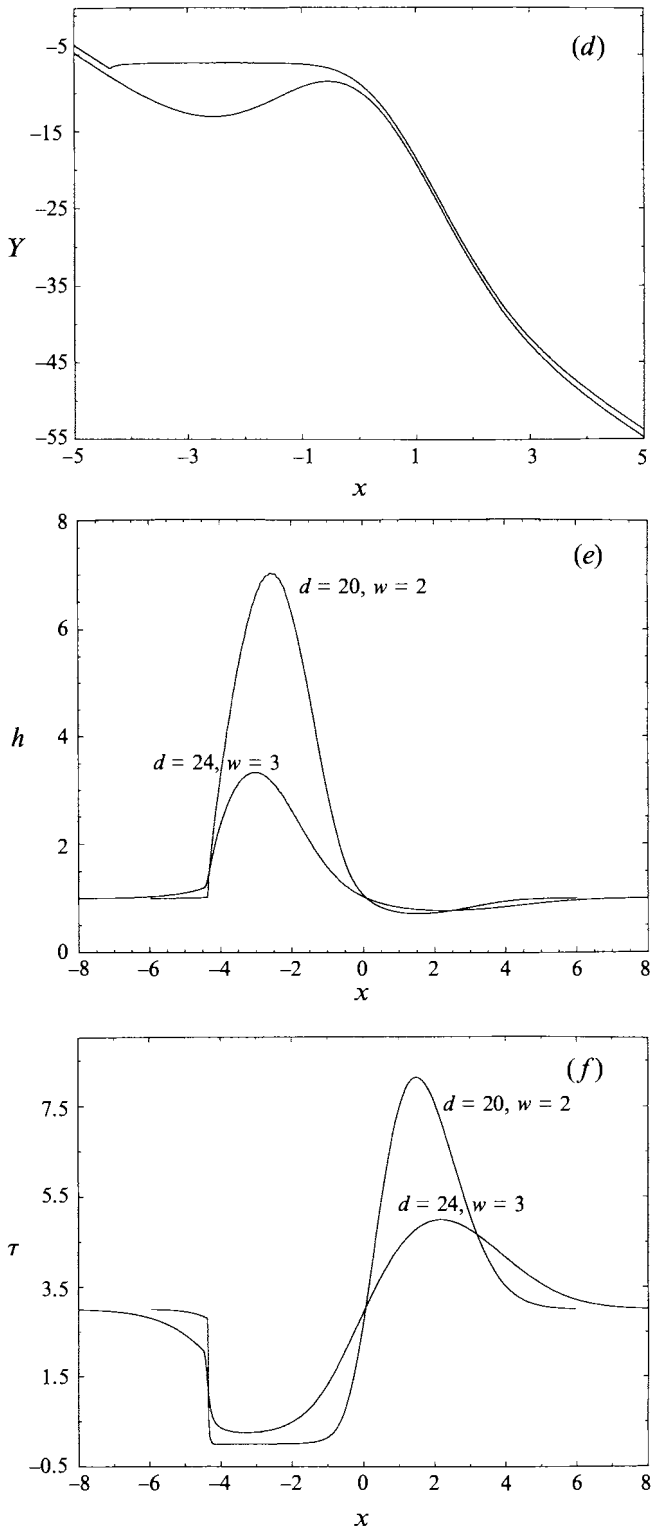

FIGURE 9. Numerical solutions of the forced interaction on slopes of $O(Re^{-1})$, showing the position of the free surface, the depth and the skin friction at the bed. See Appendix C and the text. The bed

In the experiments, a liquid layer of vegetable oil was allowed to flow over a pair of symmetrical, approximately sinusoidal, ridges placed one after the other on an otherwise uniform sloping bed. Great care was taken to ensure that the flow remained two-dimensional for as much as the channel width as possible. The slope of the bed was 0.0735 radians and on the lee slope of the ridges the slope was 0.3 radians for a distance of approximately 40 mm. The ridges were 10 mm high and the peak-to-peak separation was 100 mm. The Reynolds number was varied between 0.369 and 36.6, giving values of α (see §2.2) between 0.027 and 2.69 on the bed upstream of the first ridge and between 0.114 and 11.3 in the lee of the ridges.

If we consider the flow upstream of the first ridge we may compare the experimental results with our predictions for the flow upstream of an obstacle mounted on a small slope. The normalized height of the obstacle is proportional to $Re^{-1/3}$ since we normalize distances with the layer thickness. Thus we find that it varies from 4.6 at $Re = 0.369$ to approximately 1 at $Re = 36.6$. Thus the obstacle may be regarded as large and we should expect the flow to adjust a considerable distance upstream. This may be seen in figures 14 and 17 of PST, with an adjustment approximately 100 mm ahead of the first ridge. In addition the flow just downstream of this initial adjustment can be seen to have a horizontal free surface up to the vicinity of the crest of the first ridge, as we predict.

The flow between the two ridges may, to a certain extent, be considered as the adjustment of a fully developed flow in readiness for an obstacle on the larger slopes since the local values of α are large. The normalized obstacle height here varies from 7.4 for $Re = 0.369$ to 1.6 at $Re = 36.6$. A free interaction on the lee slope is clearly seen for $Re = 0.369$. The picture becomes less clear for larger Reynolds numbers since we cannot be sure that the flow has become fully developed half-Poiseuille flow on the lee slope before adjusting for the second ridge. The streamwise distance required for this development may be estimated as $Re\,h^*$ and although this is only 0.5 mm in the case mentioned above it is as much as 100 mm, i.e. of the order of the distance between the ridges, for the case $Re = 20.5$. For the case $Re = 7.59$, discussed below, it is approximately 28 mm and the normalized obstacle height is 2.7.

The flow on the lee of the second ridge may be considered as a flow adjusting to a change in slope. The size of the disturbance to the basic flow, i.e. the ratio of the change in depth to the upstream depth, is here independent of Re and is 0.59. This is not very large and the adjustment can be seen to start very close to the end of the lee slope. This also ties in with the upstream-influence lengthscale being very short for these larger values of α, with a maximum of approximately one half of the layer depth at $\alpha = 1.55$ ($Re = 5.03$), and decreasing like $Re\,\alpha^{-3}$ as α increases (see (2.9)). This does mean however that the flow at the base of the slope is more likely to be fully developed than would be the case if the perturbation were larger.

---

is given by $s(x)$, the grid step in the x-direction is Δx and m points are used in the normal direction, The error ϵ is defined in Appendix C and the value of $x_{\pm\infty}$ give the extent of the grid. In (*a*) and (*d*) the vertical axis is $Y = y - \alpha x + s(x)$ so that the lower curve represents the bed ($y = 0$) and the upper curve the free surface ($y = 1 + \eta + \alpha x - s(x)$). (*a*) Flow from a slope 5 (α_U) onto a slope of 0.2 (α_D) i.e. $s(x) = 4.8\,H(x)\,x \tanh bx$, $b = 2$. $\Delta x = 2.5 \times 10^{-3}$–$2.5 \times 10^{-2}$, using a stretched grid, $x_\infty = -1$, $x_\infty = 6$, $m = 22$, $\epsilon = 5 \times 10^{-2}$. (*b*) the depth for the case shown in (*a*) together with the case $s(x) = 4H(x)\,x \tanh bx$, $b = 1$, $\alpha_D = 1$. Here $\Delta x = 4.4 \times 10^{-2}$, $x_\infty = -2$, $x_\infty = 5$, $m = 22$, $\epsilon = 5 \times 10^{-2}$. (*c*) The skin friction corresponding to the curves in (*b*). (*d*) Flow on a slope $\alpha = 5$ over the ridge given by $s(x) = d\exp(-x^2/w^2)$ with $d = 20$, $w = 2$, $\Delta x = 2.5 \times 10^{-3}$–$2.5 \times 10^{-2}$, using a stretched grid, $x_\infty = -6$, $x_\infty = 5.5$, $m = 22$, $\epsilon = 5 \times 10^{-3}$. (*e*) The depth for the case shown in (*d*) together with the case $d = 24$, $w = 3$, $\Delta x = 4.4 \times 10^{-2}$, $x_\infty = -10$, $x_\infty = 10$, $m = 22$, $\epsilon = 5 \times 10^{-2}$. (*f*) The skin friction corresponding to the curves in (*e*).

We now consider the actual free-surface shape in the adjustment regions mentioned above. For the smallest value of $Re = 0.369$, the maximum value of α which is attained is 0.11 and the flow is reminiscent of the solutions of the lubrication approximation, with the free surface being concave upward throughout the adjustment. The validity of this approximation was also noted and confirmed by PST. As the Reynolds number is increased the first clear evidence of a region in which the free surface is convex upwards in the results presented by PST occurs between the ridges at measurements taken at $Re = 7.59$ ($\alpha = 2.35$). It does not seem to occur at $Re = 5.03$ ($\alpha = 1.55$), but the diagram (figure 14*b* in PST) is not very clear on this point. This compares well with the predicted value of $\alpha = 1.81$. Similar behaviour is also first seen in the adjustment ahead of the first ridge at $Re = 31.4$ ($\alpha = 2.3$) although again one might argue that it is seen at $Re = 25.5$ ($\alpha = 1.87$). These comparisons are very encouraging, especially as the theoretical predictions here arise solely from considering the free interaction and take no account of the proximity of the obstacle causing the adjustment. Although, as we mention above, the theory cannot be expected to be valid between the ridges at larger values of Re, where the flow is not fully developed, we can see that the flow here does take the general forms that we would predict as Re increases. The lengthscale of the adjustment becomes shorter and the maximum surface slopes increase. Figure 15 of PST shows the numerical results for the flow between the two ridges at $Re = 20.5$ and $Re = 25.5$ ($\alpha = 6.34$ and $\alpha = 7.88$), which agree reasonably well with the experimental results at these Reynolds numbers. These solutions exhibit jumps of the same general form as predicted in §2.3 with an initial exponential departure followed by a blunt profile with the main body of the flow being lifted off the bed, although the flow does not seem to separate. Downstream the free surface exhibits waves. We note here that even for the largest values of α, PST do not note separation of the liquid layer, either in their experimental or computational studies. We put this down to the ridge height being too small for the interactions to commence sufficiently far upstream. As a result the influence of the obstacle is soon felt by the developing flow and in particular the effective value of α is decreased by the forward facing slope of the ridge.

We now turn our attention to the waves which are seen after the jumps for the larger values of α. We predict in §2.3 that waves are possible when the parameter $\tilde{\alpha} = \tan\alpha^* Re^{5/7}$ becomes $O(1)$ as $Re \to \infty$, and that when they first appear as α^* increases they have short wavelengths, essentially being inviscid gravity waves. For larger values of $\tilde{\alpha}$ their wavelength increases and they become influenced by the effects of viscosity and a viscous–inviscid interaction. Finally if $\tilde{\alpha} Re^{-4/7}$ becomes as large as $O(1)$ the wavelength becomes effectively infinite and no waves are seen. If we concentrate on the flow on the lee of the second ridge this latter parameter is always less than 0.5 in all of the experiments reported, and again because of the small magnitude of the adjustment here the waves actually occur over the slope downstream of the ridge, effectively reducing the size of this parameter still further. We do see however that waves first occur at $Re = 12.2$ ($\tilde{\alpha} = 1.85$) and persist up to the largest Reynolds number considered, $Re = 36.6$ ($\tilde{\alpha} = 4.05$), and that the wavelength of the waves steadily increases with the Reynolds number. The behaviour is very similar to that in the solutions presented in BS for linearized flow over an obstacle on a horizontal surface as their parameter γ, equivalent to $\tilde{\alpha}$, is increased.

7. Discussion and conclusions

Throughout this work we make the assumption that the flows are steady and that the solutions we find are stable. It is well known (Benjamin 1957; Yih 1963) that half-

Poiseuille flow down an incline of slope α^* is unstable if the Reynolds number exceeds $\frac{5}{6}\cot\alpha^*$. This is formally quite a severe restriction since it implies that strictly the maximum slope for a steady flow is, in our notation, $\alpha = 5/6$. This is too small either for there to be a rise in the position of the free surface throughout the free interaction or for separation to occur and makes many of our predictions for the shape of hydraulic jumps on larger slopes strictly invalid. The work in the limit of vanishing slope remains valid. However, in the experiments of PST a slight time dependence in the experimental results was first observed, as the Reynolds number increased, between the ridges at a Reynolds number corresponding to the much larger values $\alpha \approx 10$ ($\tilde{\alpha} \approx 3.6$), so the present results are likely to be of practical value. A possible reason for this extension of the range of stability is that the disturbance which first becomes unstable as the Reynolds number or slope is increased has zero wavenumber and in any physical situation there must be some limit on the smallness of the disturbance wavenumbers that are possible. In addition the growth rates of these disturbances are small if the Reynolds number is just above critical and the effect of surface tension is to reduce these growth rates still further.

We conclude with a list of the major results of this paper.

(i) Half-plane Poiseuille flow is not a unique solution for steady flow of a liquid layer on a uniform bed. This is due to the streamwise development of eigensolutions which have their origin in interaction between the self-induced pressure gradient caused by the change in position of the free surface and viscous effects.

(ii) The lengthscale of the development of these eigensolutions is long ($O(Re)$) for shallow slopes ($O(Re^{-1})$) but decreases rapidly as the slope increases. This relatively rapid adjustment is associated with a locally strong adverse pressure gradient leading to separation of the flow from the bed and the formation of a jet beneath a horizontal free surface. We have associated this with a standing hydraulic jump.

(iii) We have made predictions for the shape of the free surface during the slower interactions on smaller slopes. Specifically the free surface is concave upwards throughout the adjustment to a horizontal downstream asymptote only for $\alpha^* < 1.814\,Re^{-1}$. Separation can occur if $\alpha^* > 4.712\,Re^{-1}$ but this is not necessarily of the breakaway type described in (ii) above unless $\alpha^* > 5.461\,Re^{-1}$.

(iv) For slopes of $O(Re^{-5/7})$ the cross-stream pressure gradient caused by streamline curvature becomes important in the interaction process, as was also found by Gajjar (1987). We have considered two effects of this. First, it can cause the free surface to be concave upwards during the interaction, if $\alpha^* \sim O(Re^{-1/7})$. Secondly, it may give rise to gravity waves downstream of the jump, as seen in the experimental and computational results of PST. These waves become longer and more subject to viscous attenuation as the slope increases.

(v) For slopes of $O(Re^{-1})$ we have presented numerical results showing that a system of interactive boundary-layer equations is capable of describing the steady flow of the layer over a large obstacle or upstream of a decrease in slope. If the slope is large, these results show a region of rapid adjustment far upstream of the obstacle, the standing hydraulic jump, and a slower scale of development as the flow passes over the obstacle. The hump is situated at a distance upstream proportional to the obstacle height. These results complement those of Higuera (1994) for flow on a horizontal surface.

(vi) On the shallowest slopes lubrication theory may be used to describe the adjustment. It is worth noting that this simple ordinary differential equation exhibits much of the behaviour seen in full interactive boundary-layer equations for $P-A$ laws that admit upstream influence, for example the emergence of a free interaction far upstream as the size of the perturbation increases.

The core elements of this work were pursued during the author's doctoral studies and thanks are due to SERC for financial support. Numerous discussions with Professor F. T. Smith are also acknowledged. Thanks are also due to the referees for their helpful comments.

Appendix A. Numerical solutions of the free interaction on $O(Re)$ lengthscales

Solutions of equation (4.1) describing the liquid-layer flow down a uniform gradient of magnitude $O(Re^{-1})$ can be obtained using the following method. Here we consider the free interaction problem.

To deal with the unknown position of the free surface we introduce the variable

$$\xi = (y-s)/h, \tag{A 1}$$

where h is the unknown depth of the layer and, in this instance, $s = 0$, since the slope is uniform. Then introducing a stream function $\Psi(x, \xi)$,

$$UU_x - \hat{\Psi}_x U_\xi/h = -p_x + U_{\xi\xi}/h^2, \quad U = \Psi_\xi/h, \tag{A 2a, b}$$

$$\Psi = U = 0 \quad \text{at} \quad \xi = 0, \quad U = 0, \quad \Psi = 1 \quad \text{at} \quad \xi = 1. \tag{A 2c–f}$$

We also have the pressure-displacement law

$$p = 3\eta/\alpha. \tag{A 3}$$

The vertical velocity V is given $-\Psi_x + (\xi h_x + s_x)\, U$.

The conditions imposed at $x = 0$ are $U = U_{PPF}(\xi)$, $V = 0$, i.e. a velocity profile given by half-Poiseuille flow in a direction parallel to the slope, and $h = 1+\delta$ where δ represents a small perturbation to the basic undisturbed flow.

The solutions are marched forward from this initial profile using a central-difference finite-difference formulation. Nonlinearity is dealt with using Newton iteration until successive iterates differ by less than 10^{-6} which takes 5 or 6 iterations using the solution at the previous x-station as an initial guess. The stepsize in x, Δx, needed to be smaller for the larger values of α to maintain accuracy and similarly the number of points in the ξ-direction, m, needed to be increased. The system is third order in ξ with an additional unknown h. The fourth boundary condition is used to determine h, using the technique described by Smith (1974). Numerically the regions of reversed flow are handled using the so-called Flare approximation (Reyner & Flügge-Lotz 1968) in which the term UU_x is set equal to zero if $U < 0$. This is an effective and, since the speed of any reversed flow is usually much less than that of forward flow, quite accurate device for obtaining solutions.

Appendix B. The effect of a large surface tension coefficient on the free interaction

Here we consider an effect surface tension has upon the compressive free interaction within the context of lubrication theory. The governing equation, including capillary effects, is from (5.1),

$$h_X - \gamma h_{XXX} = 1 - 1/h^3, \quad h \to 1 \quad \text{as} \quad X \to -\infty, \tag{B 1a, b}$$

where $\gamma (> 0)$ measures the relative importance of surface tension and $\gamma \gg 1$ if surface tension dominates. This is the limit we examine here. We can write γ as $(Re \sin\alpha^*)^{2/3} (T/\rho g^{1/3} 3^{2/3} Q^{*4/3})$ and the lubrication approximation requires $Re \sin\ \alpha^* \ll 1$ so this limit may be relevant only in reduced-gravity situations. The large-X asymptote which we expect to emerge from the interaction is still $h \sim X$.

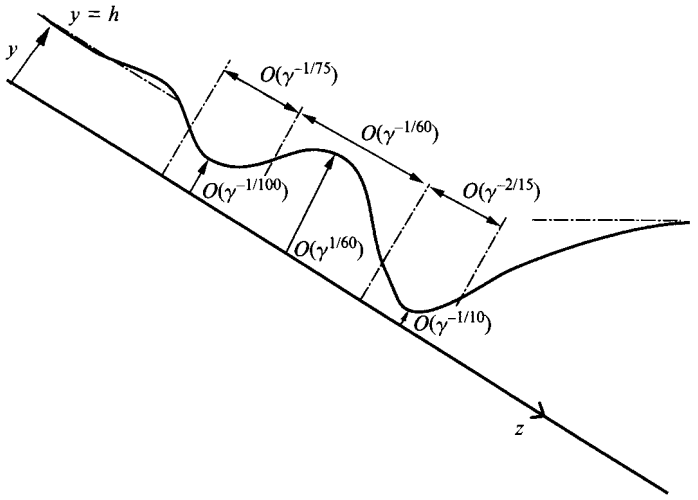

FIGURE 10. The asymptotic structure of the free interaction governed by equation (B 1) in the limit of large surface-tension coefficient γ with $z = \gamma^{-1/3}X$. A steady nonlinear wave train upstream is followed by an approach of the free surface towards a horizontal asymptote from below.

We choose a more appropriate lengthscale and write $X = \gamma^{1/3}z$, where $z = O(1)$ as $\gamma \to \infty$, to get

$$h_{zzz} - \gamma^{-1/3}h_z = 1/h^3 - 1, \quad h \to 1 \quad \text{as} \quad z \to -\infty. \tag{B 2a, b}$$

A similar equation is discussed by Wilson & Jones (1983, referred to herein as WJ) in the case of a vertical plate where the effects of the self-induced pressure gradient are identically zero but there is a small parameter entering through the denominator of the curvature term in equation (2.2*b*), which they retain. We follow much of their analysis and refer the reader there for more detail. As a first step we consider the equation with $\gamma = \infty$. WJ show that the solution in this case consists of a nonlinear wave train of successive dips, in which the depth is relatively small, and leaps, in which the depth is large. The neglected term, here the self-induced pressure gradient, re-enters in a final leap, leap 0 say. We number successive leaps, moving in an upstream direction, 1, 2, 3, ..., and the intervening dips 1, 2, 3, ... In the dips the dominant balance is between viscosity and surface tension, between the first terms on the left- and right-hand sides of (B 2*a*). As a result if the depth in the *i*th dip, moving upstream, is of size $h \sim O(\delta_i) \ll 1$, then the width of the dip is $z \sim O(\delta_i^{4/3})$. In each leap the balance is between surface tension and gravity, the first term on the left and the second term on the right of (B 2*a*). If the depth in the *i*th leap is $h \sim O(\nu_i)$ with $\nu_i \gg 1$ then the width is $z \sim O(\nu_i^{1/3})$. The equation governing the depth in the dip has two alternative asymptotes on leaving the dip, either linear or quadratic growth in h. WJ show that a wave train in which the amplitude of the waves decreases upstream can be generated by insisting that there is quadratic growth leaving the dip in a downstream direction but only linear growth leaving in an upstream direction. They show that this implies that $\delta_{i+1} = \nu_i^{-1/5} = \delta_i^{1/10}$. As a result, the amplitude of the wave train decreases rapidly upstream, giving the upstream asymptote $h \sim 1$. In practice only a few waves will be seen.

In the final leap the z-scale is so large that the neglected term becomes important. This scale is $z \sim O(\gamma^{1/6})$ so that $\nu_0 = \gamma^{1/2}$, and the scalings of all the leaps and dips upstream can be found. See figure 10. In this final leap the dominant balance is between the left-hand side and the second term on the right-hand side of (B 2*a*) so that

$h \sim \gamma^{1/2}(\gamma^{-1/6} z + B + C\exp(-\gamma^{-1/6} z))$ where the origin in z has been fixed to coincide with dip 1. As $z \to \infty$ the viscous–inviscid interaction is lost to first order and the free surface becomes horizontal with $h \sim \gamma^{1/3} z \sim X$. As $z \to 0+$ we require the depth to decrease quadratically to zero so that $B = -1$ and $C = 1$.

Appendix C. Numerical solutions of the forced interaction on $O(Re)$ lengthscales

The solutions of (4.1) in figure 9 are obtained by a relaxation procedure on η. We fix $\eta(x)$ at $\eta^n(x)$ say, impose the upstream condition $h = 1$ at $x = x_{-\infty}$ and calculate the solution to $x = x_\infty$ using a method similar to that described in Appendix A and calculating the corresponding pressure $p^n(x)$. The value of $\eta(x)$ is updated using the formula

$$\eta^{n+1} = \eta^n + \omega(\mathrm{d}/\mathrm{d}x)(3\eta^n/\alpha - p^n), \tag{C 1}$$

where ω is a relaxation parameter. The values of η at $x_{\pm\infty}$ remain unaltered. The process is repeated until a converged solution is obtained in the sense that

$$\max|p - 3\eta/\alpha| < \epsilon. \tag{C 2}$$

In all cases the procedure was started using the initial guess $h = 1$ except in the case of flow onto a different downstream slope in which case the initial guess at the depth rose smoothly to $h = (\alpha_U/\alpha_D)^{-1/3}$ at x_∞.

Typical values of ϵ used are 0.01 or 0.005, corresponding to errors of about 1% or less since a typical value of the pressure, close to the jump say in figure 9(d), is -5. The value of ω is typically small (10^{-4}) so that many iterations were needed, typically 10^5 to achieve this accuracy. Typically 22 grid points were taken in the vertical direction. The solutions presented here are believed to be grid independent to within graphical accuracy. A stretched grid in the x-direction is required to resolve the jump where the depth and skin friction vary rapidly. This grid was designed using the results from a preliminary run with a uniform grid which gave an approximate value for the jump position. Typical values for the x step, for figure 9(a) say, were 0.025 away from the jump and 0.0025 in its vicinity. Solutions on a grid which is too coarse exhibit grid-sized oscillations upstream of the jump.

REFERENCES

ABRAMOWITZ, M. & STEGUN, I. A. 1965 *Handbook of Mathematical Functions*. Dover.

BENJAMIN, T. B. 1957 Wave formation in laminar flow down an inclined plane. *J. Fluid Mech.* **2**, 554.

BOHR, T., DIMON, P. & PUTKARADZE, V. 1993 Shallow water approach to the circular hydraulic jump. *J. Fluid Mech.* **254**, 635.

BOWLES, R. I. 1990 Applications of nonlinear viscous-inviscid interactions in liquid layer flows and transonic boundary-layer transition. PhD thesis, University of London.

BOWLES, R. I. & SMITH, F. T. 1992 The standing hydraulic jump: theory, computations and comparisons with experiments *J. Fluid Mech.* **242**, 145 (referred to herein as BS).

BROTHERTON-RATCLIFFE, R. V. 1986 Boundary-layer effects in liquid-layer flows. PhD thesis, University of London.

BROWN, S. N., STEWARTSON, K. & WILLIAMS, P. G. 1974 On expansive free interactions in boundary layers. *Proc. R. Soc. Edinb.* A **74** (21), 271.

CHESTER, W. 1966 A model of the undular bore on a viscous fluid. *J. Fluid Mech.* **24**, 367.

CHRISTODOULOU, K. N. & SCRIVEN, L. E. 1989 The fluid mechanics of slide coating. *J. Fluid Mech.* **208**, 321.

CLARKE, W. 1970 Tap-splash and the hydraulic jump. *School Sci. Rev.* **152**, 67.

CRAIK, A., LATHAM, R., FAWKES, M. & GRIBBON, P. 1981 The circular hydraulic jump. *J. Fluid Mech.* **112**, 347.

DANIELS, P. G. 1992 A singularity in thermal boundary-layer flow on a horizontal surface. *J. Fluid Mech.* **242**, 419.

EAGLES, P. M. 1988 Jeffrey–Hamel boundary-layer flows over curved beds. *J. Fluid Mech.* **186**, 583.

FRAENKEL, L. E. 1962 Laminar flow in symmetric channels with slightly curved walls, I. On the Jeffrey–Hamel solutions for flow between plane walls. *Proc. R. Soc. Lond.* A **267**, 119.

GAJJAR, J. S. B. 1987 Fully developed free surface flows – liquid layer flow over a convex corner. *Computers Fluids* **15**, 337.

GAJJAR, J. & SMITH, F. T. 1983 On hypersonic self-induced separation, hydraulic jumps and boundary layers with algebraic growth. *Mathematika* **30**, 77.

HAMEL, G. 1916 Spiralförmige bewegungen zäher flüssigkeiten. *Jahrb. Deutsch. Math.*

HIGGINS, B. S. & SCRIVEN, L. E. 1979 Interfacial shape and evolution equations for liquid films and other visco-capillary flows. *Ind. Engng Chem. Fundam.* **18**, 208.

HIGUERA, F. 1994 The hydraulic jump in a viscous laminar flow. *J. Fluid Mech.* **274**, 69.

HUPPERT, H. E. 1982*a* Flow and instability of a viscous current down a slope. *Nature* **300**, 427.

HUPPERT, H. E. 1982*b* The propagation of two-dimensional and axisymmetric viscous gravity currents over a rigid horizontal surface. *J. Fluid Mech.* **121**, 43.

JEFFREY, G. B. 1915 The two-dimensional viscous motion of a steady fluid. *Phil. Mag.* **29**, 445.

LAMB, H. 1932 *Hydrodynamics*. Cambridge University Press.

LARRAS, M. 1962 Ressaut circulaire sur fond parfaitemenr lisse. *C.R. Acad. Sci. Paris* **225**, 837.

LIGHTHILL, M. J. 1953 On boundary layers and upstream influence, II. Supersonic flows without separation. *Proc. R. Soc. Lond.* A **217**, 478.

LIGHTHILL, M. J. 1978 *Waves in Fluids*. Cambridge University Press.

LISTER, J. R. 1992 Viscous flows down an inclined plane from point and line sources. *J. Fluid Mech.* **242**, 631.

MERKIN, J. H. & SMITH, F. T. 1982 Free convection boundary layers near corners and sharp trailing edges. *Z. Angew. Math. Phys.* **33**, 36.

MOFFATT, H. K. 1977 Behaviour of a viscous film on the outer surface of a rotating cylinder. *J. Méc.* **16**, 651.

PEREGRINE, D. H. 1974 Surface shear waves. *J. Hydraul. Div. ASCE.* **100**, 1215 (and Discussion in **101**, 1032 (1975)).

PRITCHARD, W. G., SCOTT, L. R. & TAVENER, S. J. 1992 Numerical and asymptotic methods for certain viscous free-surface flows. *Phil. Trans., R. Soc. Lond.* A **340** (referred to herein as PST).

RAYLEIGH, LORD 1914 On the theory of long waves and bores. *Proc. R. Soc. Lond* A **90**, 324. See also *Scientific Papers*, vol. 6, p. 250. Cambridge University Press.

REYNER, T. A. & FLÜGGE-LOTZ, I. 1968 The interaction of a shock wave with a laminar boundary-layer. *Intl. J. Non-linear Mech.* **3**, 173.

ROSENHEAD, L. 1940 The steady two-dimensional flow of a viscous fluid between two inclined plane walls. *Proc. R. Soc. Lond.* A **175**, 436.

SILVA, A. F. T. DA & PEREGRINE, D. H. 1988 Steep, steady surface waves on water of finite depth with constant vorticity. *J. Fluid Mech.* **195**, 281.

SMITH, F. T. 1974 Boundary layer flow near a discontinuity in wall conditions. *J. Inst. Math. Applics.* **13**, 127.

SMITH, F. T. 1976 Flow through constricted and dilated channels, parts 1 and 2. *Q. J. Mech. Appl. Maths.* **29**, 343.

SMITH, F. T. 1982 On the high Reynolds number theory of laminar flows. *IMA J. Appl. Maths* **28**, 207.

SMITH, F. T. & DUCK, P. W. 1977 Separation of jets and thermal boundary layers from a wall. *Q. J. Mech. Appl. Maths.* **30**, 143.

STEWARTSON, K. 1974 Multistructured boundary-layers on flat plates and related bodies. *Adv. Appl. Mech.* **14**, 147.

STEWARTSON, K. 1982 Some recent studies in triple-deck theory. In *Numerical and Physical Aspects of Aerodynamic Flows* (ed. T. Cebici), p. 129. Springer.

TUCK, E. O. & SCHWARTZ, L. W. 1990 A numerical and asymptotic study of some third-order ordinary differential equations relevant to draining and coating flows. *SIAM Rev.* **32**, 453.

WATSON, E. J. 1964 The radial spread of a liquid jet over a horizontal plane. *J. Fluid Mech.* **20**, 481.

WILSON, S. D. R. & JONES, A. F. 1983 The entry of a falling film into a pool and the air-entrainment problem. *J. Fluid Mech.* **128**, 219 (referred to herein as WJ).

YIH, C. S. 1963 Stability of liquid flow down an inclined plane. *Phys. Fluids* **6**, 321.